Targeting *de novo* lipogenesis improves gemcitabine efficacy in pancreatic ductal adenocarcinoma

Sarah E Hancock[1,2], Linda Garthwaite[1], Konstantina Harellis[1], Michael Susetio[1], Eileen Ding[2], Laura Choong[1,3], Osvaldo Contreras[3,4] Amy Nguyen[1], Josiah Lising[2], Felicia KM Hansen[5], Puttandon Wongsomboon[5], Jan Philipp Menzel[5], Berwyck LJ. Poad[5,6], Todd W Mitchell[7,8], Stephen J Blanksby[5,6] Nigel Turner[1,2,*]

[1]Cellular Bioenergetics Laboratory, Victor Chang Cardiac Research Institute, Darlinghurst, NSW, Australia

[2]Department of Pharmacology, School of Biomedical Sciences, UNSW Sydney, NSW, Australia.

[3]School of Clinical Medicine, Faculty of Medicine & Health, University of New South Wales, UNSW Sydney, Sydney, NSW, Australia

[4]Developmental and Regenerative Biology Division, Victor Chang Cardiac Research Institute, Darlinghurst, NSW, Australia

[5]School of Chemistry and Physics, Queensland University of Technology, Brisbane, QLD

[6]Central Analytical Research Facility, Queensland University of Technology, Brisbane, QLD

[7]School of Medical, Indigenous & Health Sciences, University of Wollongong, Wollongong, NSW

[8]Molecular Horizons, University of Wollongong, Wollongong, NSW, Australia

* Corresponding author. Email n.turner@victorchang.edu.au

Abbreviations

ACC acetyl-CoA carboxylase, *AMP*$^{+}$ *N*-(4-aminomethylphenyl)pyridinium, *CE* cholesteryl ester, *Cer* ceramide, *CL* cardiolipin, *CombAT* combination therapy attenuated, *CON* control, *DG* diacylglycerol, *ELOVL* elongation of very long chain fatty acid protein, *FADS2* fatty acid desaturase 2, *FAS* fatty acid synthase, *FOLFIRINOX* folinic acid, 5-fluorouracil, irinotecan and oxaliplatin; *GEMC* gemcitabine, *GEMR* gemcitabine resistant, IC_{50} half maximal inhibitory concentration, *LC-MS* liquid chromatography-mass spectrometry, *LPC* lysophosphatidylcholine, *LPE* lysophosphatidylethanolamine, *MUFA* monounsaturated fatty acid, *OzFAD* ozone-induced fatty acid discovery, *PBS* phosphate buffered saline *PC* phosphatidylcholine, *PDAC* pancreatic ductal adenocarcinoma, *PE* phosphatidylethanolamine, *PG* phosphatidylglycerol, *PS* phosphatidylserine, *PTX* paclitaxel, *PUFA* polyunsaturated fatty acid, *SCD1* stearoyl-CoA desaturase 1, *SFA* saturated fatty acid, *siRNA* small interfering siRNA *SM* sphingomyelin, *TBST* Tris-buffered saline with 0.1% Tween20, *TG* triacylglycerol, *VEH* vehicle.

Abstract

Pancreatic ductal adenocarcinoma (PDAC) is a highly aggressive disease with few treatment options and poor survivability. In this work we sought to characterise metabolic adaptations to gemcitabine (GEMC)-based chemotherapy exposure to discover new therapeutic targets for improving treatment efficacy. We show that GEMC resistance (GEMR) upregulates *de novo* lipogenesis in Panc1 and MiaPaCa2 cells through increased activity and expression of acetyl-CoA carboxylase (ACC), fatty acid synthase (FAS) and stearoyl-CoA desaturase 1 (SCD1). We also discovered alternate fatty acid desaturase 2 (FADS2) activity in Panc1 cells, which led to the production of sapienic acid (FA 16:1*n*-10, *cis*) from palmitic acid (FA 16:0). Knockdown of key lipid synthesis enzymes sensitised cells to GEMC treatment, with FAS (both cell lines), SCD1 (MiaPaCa2 only) and SCD1+FADS2 (Panc1) knockdown showing the greatest reduction in cell growth when combined with GEMC treatment. In Panc1 cells, either desaturase upregulated its activity when the alternate was knocked down, necessitating the need for dual desaturase knockdown in this cell line. PDAC cells attenuated to grow in combination GEMC/paclitaxel (CombAT) also displayed enhanced *de novo* lipogenesis; however, combination chemotherapy significantly downregulated FADS2 expression and activity in Panc1 CombAT cells rendering them more sensitive to SCD1 knockdown. We conclude that co-targeting lipid synthesis in PDAC could be a viable strategy for improving the efficacy of both GEMC monotherapy and combination GEMC/PTX therapy.

Introduction

Pancreatic ductal adenocarcinoma (PDAC) is the twelfth most common cancer worldwide, with close to half a million new cases being diagnosed in 2020 (1). Despite its relatively low incidence rate, the mortality associated with PDAC remains high, with a global 5-year overall survival rate of just 9% (2). The ongoing poor survivability of PDAC is a result of many contributing factors. PDAC is a highly asymptomatic disease that is often detected at later stages, with fewer than 20% of cases being eligible for surgical resection at the time of diagnosis (3). For most patients only palliative chemotherapy remains as a treatment option. Either FOLFIRINOX (folinic acid, 5-fluorouracil, irinotecan and oxaliplatin) or gemcitabine (GEMC) monotherapy have long been the primary chemotherapy options for PDAC, with the former coming at a cost of higher toxicity (4,5). More recently, GEMC combined with albumin-bound (nab-)paclitaxel (also known as Abraxane) has replaced GEMC monotherapy as the standard of care for metastatic PDAC, but survivability still remains extremely poor with an increase in median overall survival of only a few months when compared with GEMC monotherapy (6).

Underlying the poor treatability and chemoresistance of PDAC are a myriad of genetic mutations, many of which are sporadic and heterogeneous between patients. Activating mutations in *KRAS* are common and present in around 90% of tumours, as are inactivating mutations in *TP53*, *CDKN2A*, and *SMAD4* (>20% of tumours) (3,7). Beyond this, common mutations seen across PDAC tumours drop to <10% (3,8), precluding the identification of druggable gene therapy targets that can impact a majority of patients. The genetic mutations present in PDAC have wide-ranging impacts on tumour molecular biology, activating diverse pro-survival and anti-apoptotic signalling pathways (9–11). Further compounding the chemoresistant nature of PDAC is the presence of a dense desmoplastic stroma that creates a hypoxic tumour microenvironment and impedes the delivery of chemotherapy to cancer cells (12). Together this results in extensive metabolic reprogramming in PDAC to facilitate the acquisition of biomolecules necessary to support cancer cell rapid growth and proliferation. Despite the lack of a good genetic therapeutic target in PDAC, mutational effects likely converge on relatively fewer metabolic pathways (13,14), making metabolism-based therapies an attractive pathway for improving options for PDAC treatment.

The role of lipid metabolism in cancer cell survival, metastasis, and chemoresistance has become a recent topic of interest across many different cancer types including PDAC (15–21). Lipids are ubiquitous molecules essential to life that have diverse functions in biology, including in energy production and storage, cell signalling, as structural components of cell membranes that can also modulate membrane-bound proteins, as well as substrates for post-translational modifications. The diversity of biological function in lipids is reflected by their complex and varied structures, as their structural composition typically informs their biology. Key *de novo* lipogenesis enzymes are commonly upregulated in many cancers, consistent with the continual need for accrual of lipids in cancer (22). For

89 example, fatty acid synthase (FAS) is the rate-limiting step in fatty acid synthesis and catalyses the
90 elongation of malonyl-CoA produced by acetyl-CoA carboxylase (ACC) to palmitic acid (*i.e.*, FA 16:0,
91 a fatty acid with 16 carbons and no carbon-carbon double bonds). FAS is commonly expressed at high
92 levels in a variety of cancers (reviewed by (23–25)), where its overexpression often correlates to poorer
93 survival (17,26) and chemotherapy resistance (17,27–29). Aberrant lipid metabolism is an emerging
94 metabolic hallmark of PDAC, where fatty acid and sterol metabolism is upregulated (18,30), and
95 distinct lipid signatures can predict patient prognosis and resistance to chemotherapy PDAC (15).
96 Collectively, relatively little is known about the role of lipid metabolism in PDAC growth, metastasis,
97 and chemoresistance, and therefore a more complete elucidation of implicated metabolic pathways
98 could lead to the identification of novel therapeutic targets to improve PDAC treatment and patient
99 survival.

100 In this work, we describe significant increases in *de novo* lipogenesis following chronic treatment of
101 PDAC cells with GEMC monotherapy or combination GEMC/paclitaxel (PTX) therapy. We show that
102 targeting key lipogenic enzymes can improve the efficacy of GEMC chemotherapy, including ACC1,
103 FAS, stearoyl-CoA desaturase 1 (SCD1) and fatty acid desaturase 2 (FADS2). Furthermore, we describe
104 Δ6 desaturation of saturated fatty acids by FADS2 in PDAC for the first time, alongside selective
105 downregulation of FADS2 by chronic GEMC/PTX treatment offering a novel pathway towards dual
106 desaturase targeting to improve GEMC-based chemotherapy efficacy in PDAC.

107 Results

108 Development of GEMR PDAC cell lines

109 Panc1 and MiaPaCa2 were chosen as model cell lines to explore chemotherapy-induced metabolic
110 reprogramming due to their divergent mutational heterogeneity (Figure S1) combined with discrete
111 metabolic phenotypes (31). Generation of gemcitabine resistant (GEMR) cell lines was achieved by
112 culturing Panc1 and MiaPaCa2 cells in increasing doses of GEMC over a period of 10-12 weeks. The
113 cells were deemed resistant once a difference in the half maximal inhibitory concentration (IC_{50}) could
114 be observed between treated and non-treated control (CON) cells. Panc1 cells were attenuated to grow
115 150 nM GEMC and MiaPaCa2 in 64 nM, and at the final concentration of GEMC, Panc1 GEMR cells
116 had an IC_{50} for GEMC that was more than 2.5 times that of CON Panc1 cells (Table 1), with the IC_{50}
117 of MiaPaCa2 GEMR cells being just over 3 times that of CON. Proliferation in Panc1 GEMR cells was
118 slightly increased compared with controls, with CON cells having a doubling time of 1.30 (1.07-1.57,
119 95% CI) days compared with GEMR at 0.97 (0.78-1.21, 95% CI) days. (Figure S2A). In contrast, the
120 doubling time of MiaPaCa2 cells were similar between CON and GEMR cells, being 1.33 (1.18-1.49,
121 95% CI) and 1.32 (1.21-1.45, 95% CI) days, respectively. Few overt morphological changes could be
122 observed in either cell line when GEMR was compared with CON (Figure S2B). Together these data

123 suggest that both PDAC cell lines are newly adapted to GEMC, with none of the typical more extreme
124 changes in cell morphology or growth rate seen in more advanced GEMR PDAC models (32–34).

125 **Table 1:** half-maximal inhibitory concentration of control and gemcitabine-resistant (GEMR) PDAC
126 cell lines.

Cell line	IC_{50} (nM)	95% CI (nM)	p value*
Panc1 CON	273.3	136.0 - 575.5	-
Panc1 GEMR	720.5	427.2 - 1225.0	0.012
MiaPaCa2 CON	30.6	20.3 - 46.1	-
MiaPaCa2 GEMR	92.2	59.7 - 142.2	<0.001

127 *CON* control *GEMR* gemcitabine resistant IC_{50} half-maximal inhibitory concentration.
128 * control vs GEMR, non-linear regression with extra sum-of-squares F test, n= 3.
129

130 **GEMR alters lipid profile and increases lipid droplet number in Panc1 cells**

131 Previous work had indicated a distinct lipidomic signature associated with chemoresistant PDAC (15),
132 and so to better understand the changes that might be occurring in PDAC cell lipid metabolism with
133 GEMR we performed untargeted lipidomics using liquid chromatography-tandem mass spectrometry
134 (LC-MS/MS). Untargeted lipidomics enabled the quantification of more than 400 distinct molecular
135 lipid species within Panc1 & MiaPaCa2 control & GEMR cells from 12 different classes of lipid,
136 including cholesteryl esters (CE), ceramides (Cer), cardiolipin (CL), diacylglycerol (DG),
137 lysophosphatidylcholine (LPC), lysophosphatidylethanolamine (LPE), phosphatidylcholine (PC),
138 phosphatidylethanolamine (PE), phosphatidylglycerol (PG), phosphatidylserine (PS), sphingomyelin
139 (SM) and triacylglycerol (TG). Of these 400-plus molecular lipids species, 77 displayed statistically
140 significant differences ($P < 0.05$) between Panc1 control and GEMR cells (Figure 1A), with 79
141 statistically significant differences detected between the two MiaPaCa2 cell lines (Figure 1B). While
142 there appeared to be roughly equal proportions of increased and decreased lipid species between Panc1
143 CON & GEMR cells (Figure 1A), lipid species in MiaPaCa2 GEMR cells were mostly decreased when
144 compared to CON (Figure 1B). Interestingly, Panc1 cells appeared to have an overrepresentation of
145 lipids containing saturated (no carbon-carbon double bonds; SFA) or monounsaturated fatty acids (1
146 carbon-carbon double bond; MUFA) that were increased with GEMR (Figure 1A), strongly suggesting
147 the upregulation of *de novo* lipid synthesis within this cell line. Confocal imaging of BODIPY-stained
148 cells revealed increased lipid droplet number per cell in Panc1 GEMR cells when compared with CON,
149 with no change in lipid droplet size (Figure 1D). No significant change in lipid droplet number or size
150 was observed between MiaPaCa2 CON and GEMR cells (Figure 1E); however, MiaPaCa2 CON cells
151 contained approximately three times more neutral lipid droplets per cell compared with Panc1 CON
152 (Figure 1F). Together these data suggest a role for GEMC-driven upregulation of *de novo* lipogenesis
153 and lipid droplet biogenesis in Panc1 cells specifically.

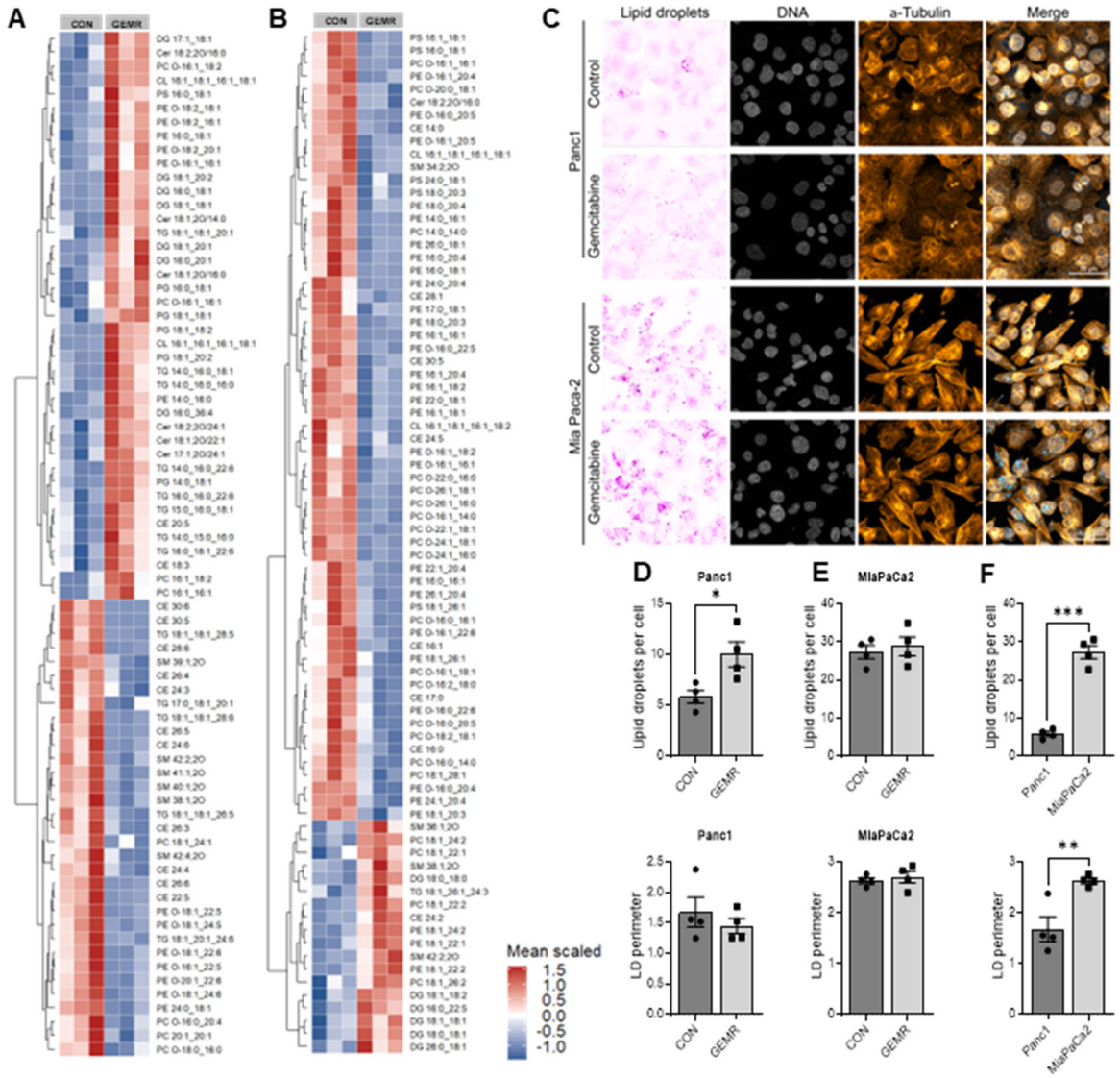

Figure 1: Differentially abundant lipid species from **A** Panc1 and **B** MiaPaCa2 CON & GEMR cell lines detected by untargeted lipidomics (unpaired t test, $P < 0.05$). Lipids were quantified from internal standards, and values are mean-scaled. **C** Representative confocal images of BOPIDY-stained Panc1 & MiaPaCa2 CON & GEMR cells lines, with (**D-E**) quantification of lipid droplets per cell and lipid droplet perimeter (µm). **F** Comparison of lipid droplet number and size between Panc1 and MiaPaCa2 cells. Statistical significance was determined by unpaired t test, *$P < 0.05$ ** $P < 0.01$. *** $P < 0.001$

GEMR increases *de novo* lipogenesis in PDAC cell lines

To better understand GEMR-driven reprogramming of PDAC lipid metabolism we undertook extensive profiling of lipid synthesis pathways in both cell lines (Figure 2A). We measured *de novo* lipogenesis in PDAC cells by tracing the incorporation of radiolabelled glucose into the lipid fraction of both Panc1 and MiaPaCa2 CON & GEMR cells (Figure 2B). Surprisingly GEMR increased *de novo* synthesis of lipid from glucose in both PDAC cell lines, despite MiaPaCa2 GEMR cells showing fewer increases in lipid species (Figure 1B) and no change in lipid droplet size or number when compared with CON (Figure 1C&E). To further elucidate specific changes in lipid metabolism we next performed

169 immunoblotting to characterise changes in total and activated enzymes involved in lipid synthesis.
170 Acetyl-CoA carboxylase 1 (ACC1) catalyses the first step of fatty acid synthesis, forming malonyl-
171 CoA (Figure 2A). Phosphorylation of ACC1 at serine 79 inhibits ACC1 activity, and palmitic acid (FA
172 16:0) is synthesised by fatty acid synthase (FAS) by the sequential elongation of ACC1-derived
173 malonyl-CoA. From here, palmitic acid can be alternatively elongated by various elongation of very
174 long chain fatty acids protein (ELOVL) isoforms or desaturated (*i.e.*, the introduction of a carbon-
175 carbon double bond) to form a variety of SFA or MUFA (Figure 2A) (35,36). In Panc1 GEMR cells we
176 observed the activation of lipid synthesis pathways through decreased phosphorylation of ACC1 and
177 increased expression of FAS. MiaPaCa2 GEMR cells demonstrated a statistically significant increase
178 in total ACC1 abundance as compared to CON (Figure 2D). Together these data suggest that GEMR
179 causes upregulation of *de novo* lipogenesis in both PDAC cell lines.

180

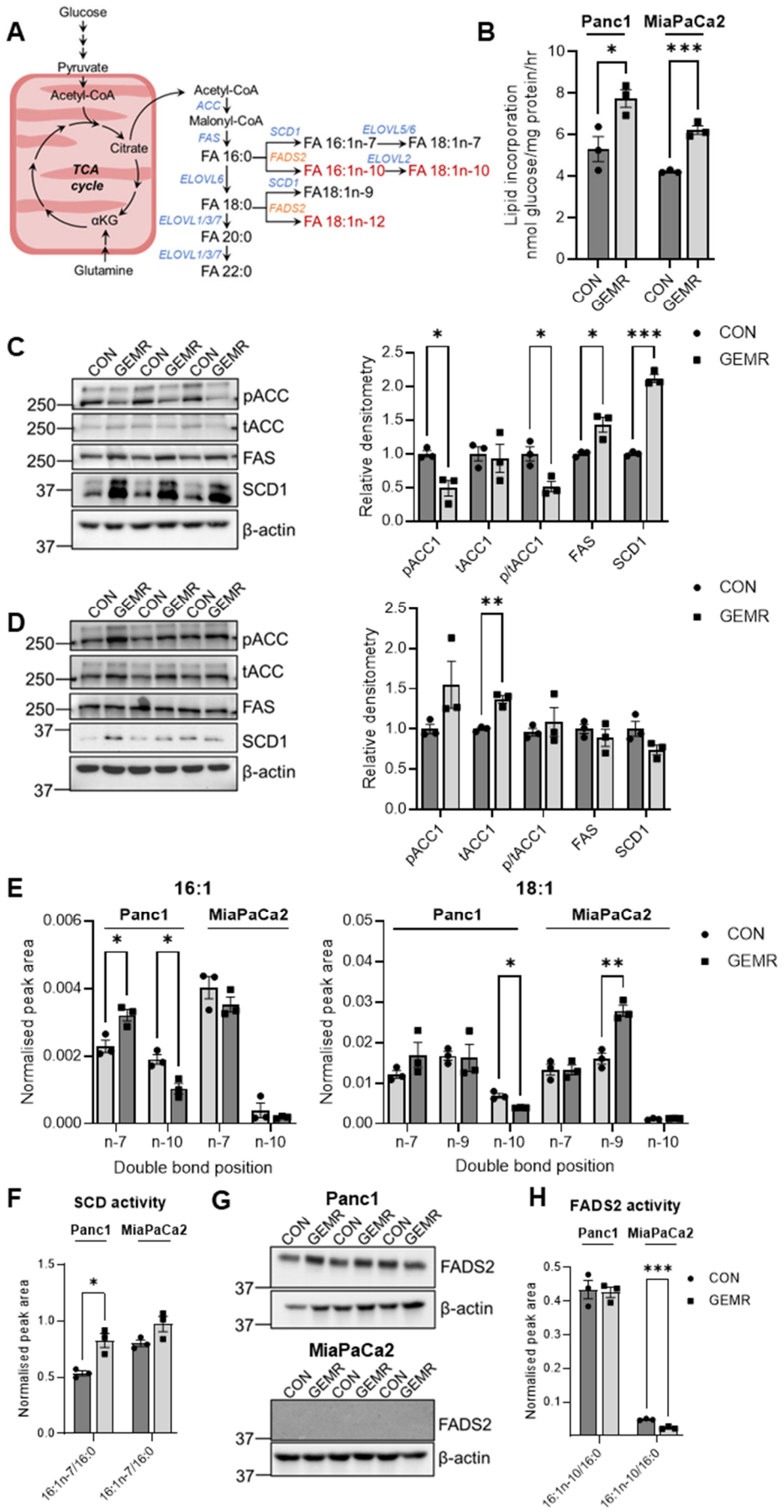
A
Glucose
Pyruvate
Acetyl-CoA
Citrate
TCA cycle
αKG
Glutamine
Acetyl-CoA
ACC
Malonyl-CoA
FAS
FA 16:0
ELOVL6
FA 18:0
ELOVL1/3/7
FA 20:0
ELOVL1/3/7
FA 22:0
SCD1
FA 16:1n-7
ELOVL5/6
FA 18:1n-7
FADS2
FA 16:1n-10
ELOVL2
FA 18:1n-10
SCD1
FA18:1n-9
FADS2
FA 18:1n-12
B
Panc1
MiaPaCa2
Lipid incorporation
nmol glucose/mg protein/hr
CON
GEMR
C
pACC
tACC
FAS
SCD1
β-actin
Relative densitometry
pACC1
tACC1
p/tACC1
FAS
SCD1
D
E
16:1
18:1
Normalised peak area
Double bond position
n-7
n-9
n-10
F
SCD activity
16:1n-7/16:0
G
FADS2
H
FADS2 activity
16:1n-10/16:0

181

182 **Figure 2: A** map of lipid synthesis in mammalian cells, including elongation and desaturation steps.
183 Canonical lipid synthesis pathways are shown in blue/black, while the alternative fatty acid desaturase
184 2 (FADS2)-mediated pathway is shown in red/orange. **B** *De novo* lipogenesis measured by tracing
185 uniformly radiolabelled glucose into the lipid fraction of control (CON) and gemcitabine resistant
186 (GEMR) Panc1 and MiaPaCa2 cells. Immunoblotting of key enzymes involved in *de novo* lipid
187 synthesis in **C** Panc1 and **D** MiaPaCa2 CON and GEMR cell lines. **E** Analysis of AMP^+-derivatised
188 isomeric FA16:1 and FA 18:1 MUFA by ozone-enabled fatty acid discovery (OzFAD). **F** SCD1 activity
189 measured by tracing uniformly labelled ^{13}C-palmitate (FA 16:0) into palmitoleic acid (FA 16:1*n*-7)
190 using liquid chromatography-mass spectrometry (LC-MS). **G** immunoblotting of FADS2. **H** FADS2
191 activity measured by tracing uniformly labelled ^{13}C-palmitic acid into sapienic acid (FA 16:1*n*-10) by
192 LC-MS. Unpaired t test, * $P < 0.05$, ** $P < 0.01$, *** $P < 0.001$. *ELOVL* elongation of very long chain
193 fatty acids *FADS2* fatty acid desaturase *FAS* fatty acid synthase 2 *pACC* phosphorylated acetyl-CoA
194 carboxylase *SCD1* stearoyl-CoA desaturase 1 *tACC* total ACC.

195 **GEMR increases stearoyl-CoA desaturase (SCD)-driven desaturation in Panc1 cells**

196 Palmitic acid can either be elongated by various ELOVL isoforms or desaturated to form MUFA (Figure
197 2A). SCD1 is an endoplasmic reticulum-localised enzyme that introduces a carbo*n*-carbon double bond
198 at the Δ9 position (*i.e.*, ninth carbon from the carboxylate end) on either palmitic or stearic acid to form
199 palmitoleic (FA 16:1*n*-7, *cis*) or oleic acid (FA 18:1*n*-9, *cis*) respectively (where the *n-x* refers to the
200 location of the carbon-carbon double bond, *x*, from the methyl end of the fatty acid with *n* carbons).
201 From here, FA 16:1*n*-7 can also be elongated by ELOVL5/6 to produce vaccenic acid (FA 18:1*n*-7, *cis*)
202 (35,36). To better understand upregulation of lipid metabolism in our GEMR PDAC cells we performed
203 immunoblotting for SCD1 (the dominant human isoform) in both cell lines and found increased
204 abundance of SCD1 in Panc1 GEMR cells by immunoblot (Figure 2C). This increase in SCD1 protein
205 abundance could explain increased levels of MUFA-containing lipids in Panc1 GEMR cells; however,
206 recent work has demonstrated the presence of FADS2-derived isomeric MUFA in other cancer types
207 (35,37) that contain carbon-carbon double bonds at locations distinct from SCD1-derived MUFA
208 (Figure 2A). Such isomers are unable to be differentiated using the LC-MS/MS method used for
209 untargeted lipidomics analysis in Figure 1A&B. To measure SCD1-derived fatty acids specifically in
210 our GEMR PDAC cell lines we performed ozone-enabled fatty acid discovery (OzFAD) (38) on AMP^+-
211 derivatised MUFA (Figure 2E). These data demonstrated a statistically significant increase in FA 16:1*n*-
212 7 in Panc1 GEMR when compared with Panc1 CON cells whereas FA 18:1*n*-9 was increased in
213 MiaPaCa2 GEMR cells. Both of these fatty acid species are SCD1-derived MUFA. (Figure 2A). To
214 confirm these findings, SCD1 activity was measured in both cell lines by measuring desaturation of
215 uniformly labelled $^{13}C_{16}$ palmitate into $^{13}C_{16}$-FA 16:1*n*-7 after 72 h. Baseline levels of FA 16:0 were not
216 different between CON and GEMR cells of either cell line (Figure S3A&B). Despite no change in
217 labelled palmitate uptake in Panc1 cells (Figure S3C), an increase in the ratio of FA 16:1*n*-7/FA 16:0
218 was detected in GEMR Panc1 cells indicating enhanced SCD1 activity in this cell line (Figure 2F). In
219 contrast, no difference was observed in SCD1 activity for GEMR MiaPaCa2 cells despite a slight
220 increase in labelled palmitate uptake (Figure S3D) and increased 18:1*n*-9 in this cell line (Figure 2E).

221 Taken together, these data suggest that GEMR upregulates SCD1 expression and activity specifically
222 in Panc1 cells.

223 Given that GEMR cells from both lines exhibited increases in *de novo* lipogenesis (Figure 2B), we also
224 sought to characterise the impact of GEMR on the utilisation of fatty acids by assessing fatty acid
225 oxidation (FAO) in both cell lines using radiolabelled palmitate. These data demonstrated a significant
226 increase in FAO in Panc1 GEMR cell lines as compared to CON, with very low rates of FAO in both
227 CON and GEMR MiaPaCa2 cells (Figure S4A). No change was observed in either GEMR cell line for
228 radiolabelled palmitic acid uptake when compared with CON (Figure S4B).

229 FADS2-derived monosaturated fatty acids are present in Panc1 cells

230 Through OzFAD we were also able to detect the presence of *n*-10 isomers of FA 16:1 and FA 18:1 in
231 both cell lines, with a greater amount of *n*-10 found in Panc1 cells relative to MiaPaCa2 (Figure 2E).
232 The amount of 16:1*n*-10 & 18:1*n*-10 detected in Panc1 GEMR cells was lower compared with CON,
233 with no change in 16:1*n*-10 or 18:1*n*-10 detected between MiaPaCa2 CON & GEMR cell lines.
234 Alternative FADS2-mediated desaturation of SFA has recently been described within prostate cancer
235 (35) and immortalised lung and breast cancer cell lines (37), where FA 16:0 is desaturated to form
236 sapienic acid (FA 16:1*n*-10, *cis*) or FA 18:0 is desaturated to petroselinic acid (FA 18:1*n*-12, *cis*; Figure
237 2A). Subsequent elongation of FA 16:1*n*-10 by ELOVL2 produces FA 18:1*n*-10 (35,36). In mammalian
238 cells FADS2 normally desaturates polyunsaturated fatty acids (PUFA; >1 carbon-carbon double bond)
239 at the Δ6 or Δ8 carbon. Immunoblotting for FADS2 revealed no difference in its abundance between
240 Panc1 CON and GEMR cells; however, FADS2 protein was virtually undetectable in MiaPaCa2 cells
241 (Figure 2G). Absence of significant FADS2 protein in MiaPaCa2 cells agrees with the much lower
242 amounts of *n*-10 fatty acids detected in MiaPaCa2 when compared with Panc1 (Figure 2E). Only trace
243 amounts of *n*-12 isomers were detected in the Panc1 cell lines (data not shown), suggesting a specific
244 upregulation of desaturation of FA 16:0 by FADS2. To further elucidate the effect of GEMR on FADS2
245 we measured its steady-state activity by tracing uniformly labelled ^{13}C palmitate into 16:1*n*-10 in both
246 cell lines. We detected no change in FADS2 activity observed between CON and GEMR Panc1 cells
247 and a small but statistically significant decrease in FADS2 activity in MiaPaCa2 GEMR cells (Figure
248 2H). Overall, these data suggest that there is no specific increase in FADS2 abundance or *n*-10 MUFA
249 synthesis activity with GEMR in either cell line.

250 SCD1 and FADS2 compensate for each other when the alternate is knocked down in 251 Panc1 cells

252 To investigate if targeting lipid synthesis can improve the response of PDAC cells to GEMC treatment
253 we performed knockdown of key enzymes using small interfering RNA (siRNA). We targeted the genes
254 of key enzymes in lipid synthesis pathways including *ACACA* (*i.e.*, the gene encoding ACC1), *FASN*

(FAS), *SCD* (SCD1), and *FADS2*. We tested single siRNA targets against *ACACA* and *FASN* and confirmed knockdown in Panc1 & MiaPaCa2 cells (Figure 3A). Knockdown of either *ACACA* or *FASN* also resulted in large decreases in *de novo* lipogenesis as measured by tracing radiolabelled glucose into the lipid fraction of CON Panc1 & MiaPaCa2 cell lines (Figure 3B). Two different siRNA targets were tested for *SCD* and *FADS2*, with either showing good efficacy in the knockdown of their target (Figure 3C). Therefore, both siRNAs for *SCD* and *FADS2* were used in combination throughout.

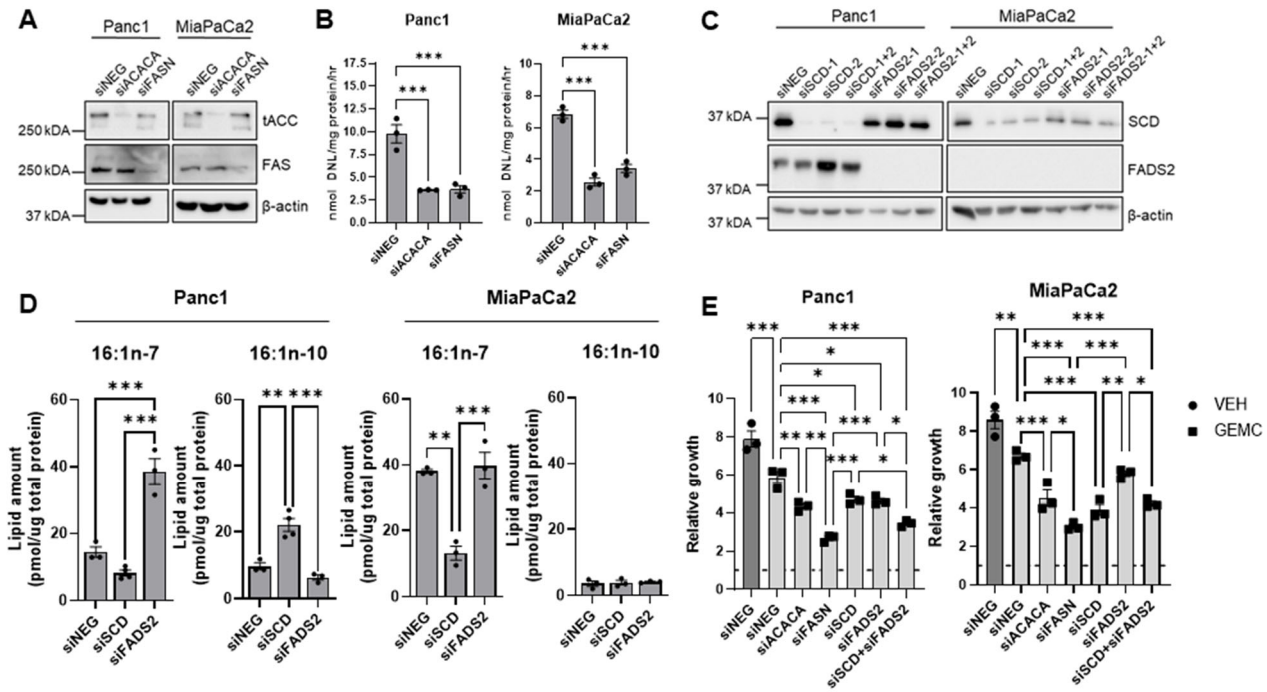

Figure 3: A Immunoblotting for ACC & FAS and **B** measurement of radiolabelled glucose into lipid fraction following knockdown of *ACACA* or *FASN*. **C** Immunoblotting for SCD1 & FADS2 or **D** quantification of 16:1 isomers measured by liquid chromatography-mass spectrometry following knockdown of *SCD* or *FADS2*. All measurements were performed following 72 h of siRNA transfection. **E** effect of 48 h GEMC treatment (Panc1 1 µM, MiaPaCa2 100 nM, or vehicle, VEH) on relative cell growth following 72 h knockdown of lipid synthesis enzymes. Cell growth was measured by crystal violet assay and normalised to start of siRNA knockdown (dashed line). Statistical significance was determined by **B** unpaired t test, or **D&E** one-way ANOVA with Tukey posthoc correction, *$P < 0.05$ ** $P < 0.01$. *** $P < 0.001$

We next measured the effect of siRNA knockdown on SCD1 and FADS2 activity by measuring changes in the amount of FA 16:1 isomers by LC-MS/MS (Figure 3D). In MiaPaCa2 cells, SCD1 knockdown had the intended effect where it significantly decreased FA 16:1*n*-7 levels. Knockdown of FADS2 in MiaPaCa2 cells did not affect the amount of FA 16:1*n*-10; however, levels of FA 16:1*n*-10 (Figure 2E) and the abundance of FADS2 protein (Figure 2G&3C) are very low in this cell line. In contrast, knockdown of either desaturase in Panc1 cells did not result in a significant decrease in the expected isomeric MUFA product; instead, the alternate desaturation product increased in abundance (Figure 3D). For example, knockdown of SCD1 in Panc1 cells resulted in a large increase in FA 16:1*n*-10 with

279 no change in FA 16:1*n*-7 content relative to si*NEG*. Likewise, the knockdown of FADS2 resulted in a
280 large increase in FA 16:1*n*-7. Together these data suggest that each desaturase can compensate when
281 the alternate is inhibited in Panc1 cells.

282 **Knockdown of lipogenic enzymes improves GEMC efficacy in PDAC cells**

283 Post validation of knockdown targets, we assessed if reducing the activity of the different lipid enzymes
284 could improve GEMC chemotherapy efficacy on cell growth in Panc1 & MiaPaCa2 cells (Figure 3E).
285 Target enzymes were knocked down in Panc1 & MiaPaCa2 cells for 72 h prior to 48 h of treatment
286 with vehicle (VEH) or a dose of GEMC tailored to induce a statistically significant decrease in si*NEG*
287 cell growth (Panc1 1 μM, MiaPaCa2 100 nM). Knockdown of *ACACA*, *FASN*, *SCD* or *FADS2*
288 combined with GEMC treatment resulted in decreased cell growth in Panc1 cells when compared with
289 GEMC-treated si*NEG* controls, with si*FASN* producing the greatest effect (Figure 3E). *ACC, SCD* or
290 *FADS2* knockdown each had an equivalent impact on cell growth. However, co-targeting desaturases
291 using si*SCD* and si*FADS2* produced a significantly greater decrease in Panc1 cell growth than targeting
292 either enzyme alone, with the effect of dual desaturase knockdown on cell growth being comparable to
293 that of si*FASN* (Figure 3E). All reported decreases in cell growth following concomitant knockdown
294 and GEMC treatment was above that for knockdown alone for all targeted lipogenic genes except *FASN*,
295 which had a similar impact on growth with or without GEMC treatment (Figure S5A). Knockdown of
296 key lipid synthesis enzymes in combination with GEMC treatment in MiaPaCa2 cells showed a similar
297 trend to that of Panc1, except that si*FASN* or si*SCD* produced a comparable decrease in relative cell
298 growth (Figure 3E). Knockdown of *FADS2* did not significantly decrease cell growth in MiaPaCa2
299 cells, which is consistent with the observed low level of FADS2 enzyme abundance (Figure 2G&3C)
300 and activity (Figure 2H&3D) in this cell line. Not surprisingly, co-targeting both desaturases with si*SCD*
301 and si*FADS2* in MiaPaCa2 cells produced no additional effect when compared with si*SCD* alone
302 (Figure 3E). The effect of combined knockdown with GEMC treatment was above that of knockdown
303 only for *ACACA* and *FASN* in MiaPaCa2 cells (Figure S5B).

304 We also measured the effect of knockdown of lipid synthesis enzymes in GEMR cells; however, only
305 si*FASN* resulted in decreased cell growth on either cell line (Figure S5C&D). Collectively, these data
306 suggest that targeting key enzymes involved in fatty acid synthesis can successfully sensitise GEMC-
307 naïve PDAC cells to GEMC treatment, and that where alternate desaturase activity exists co-targeting
308 both desaturases is necessary to have the greatest impact on cell growth.

309 **Combination GEMC/paclitaxel resistance also upregulates lipid synthesis**

310 GEMC monotherapy has long been the first-line treatment for metastatic PDAC, but is now more
311 typically given in combination with nab-paclitaxel (39). To test the effect of combination chemotherapy
312 on *de novo* lipogenesis in PDAC we chronically exposed Panc1 and MiaPaCa2 cells to
313 GEMC/paclitaxel (PTX) for 12 weeks using a similar regime to that of GEMR induction. GEMC and

314 PTX were provided to cells at a ratio of 10:1 (GEMC:PTX) to approximate the typical ratio of the two
315 drugs as given to PDAC patients (40,41). In Panc1 cells we attenuated the dose of combination therapy
316 given to a maximum of 28 nM GEMC (2.8 nM PTX), while MiaPaCa2 cells were attenuated to grow
317 in up to 8 nM GEMC (0.8 nM PTX). Combination therapy attenuated (CombAT) Panc1 and MiaPaCa2
318 cells showed improved growth and proliferation in media containing 15 nM GEMC/1.5 nM PTX when
319 compared to naïve control cells, suggesting that resistance was present in both cell lines (Figure S6).

320 We next performed untargeted lipidomics to determine relative changes in lipid species across both cell
321 lines (Figure 4A&B). These data revealed extensive increases across 166 lipid species in Panc1
322 CombAT cell lines compared with CON ($p < 0.05$), including increases in many TG species as well as
323 total TG (Figure 4A). Increases were also seen in several TG species in CombAT MiaPaCa2 cells, with
324 30 lipid species increased in total when compared with CON ($p < 0.05$; Figure 4B). Together these data
325 suggest that the addition of PTX to GEMC treatment does not abrogate the lipogenic phenotype
326 observed with monotherapy GEMR, and in fact, may enhance *de novo* lipogenesis in both cell lines.

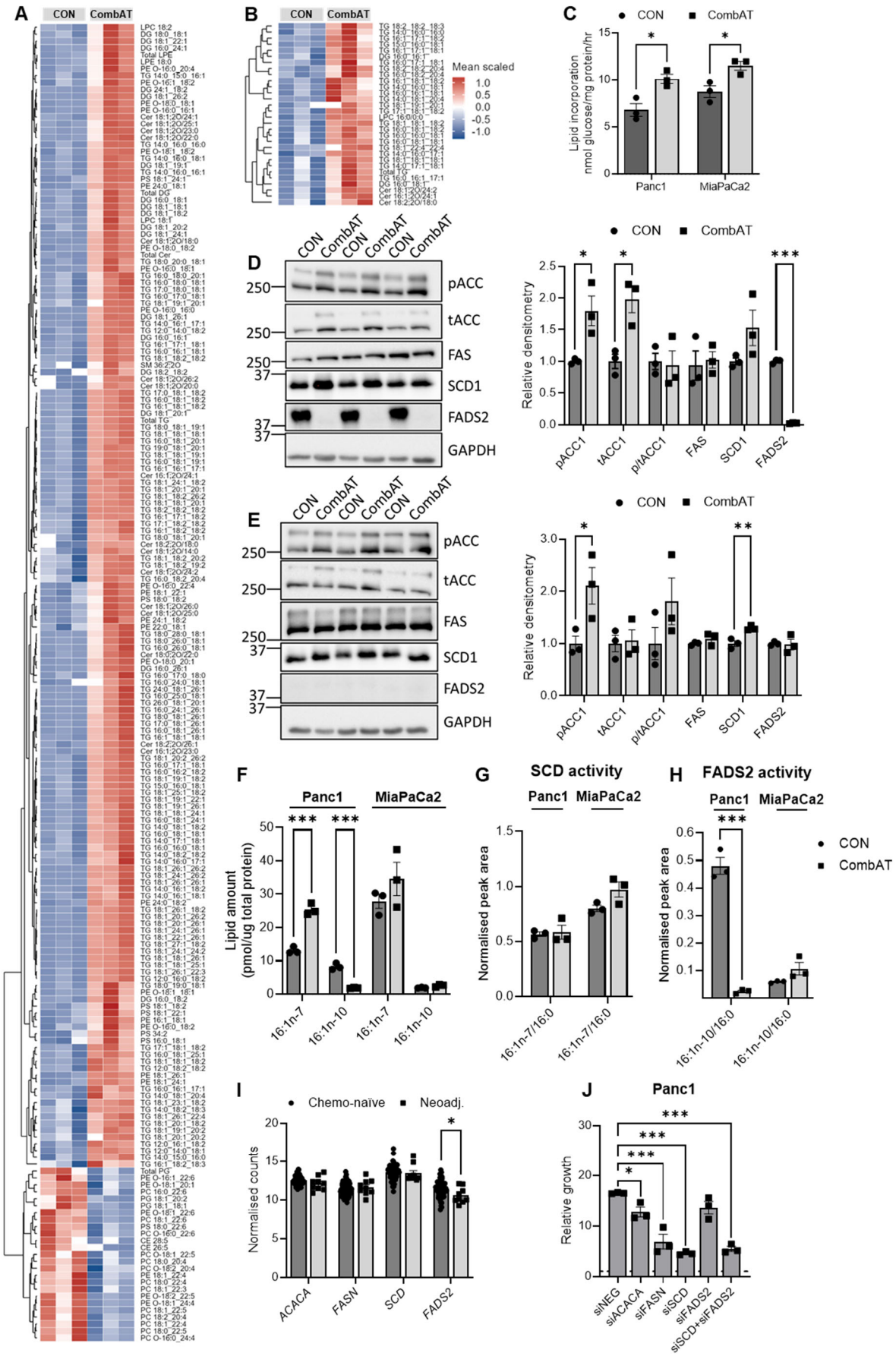
A
CON
CombAT
B
CON
CombAT
Mean scaled
1.0
0.5
0.0
-0.5
-1.0
C
CON
CombAT
Lipid incorporation
nmol glucose/mg protein/hr
Panc1
MiaPaCa2
D
CON
CombAT
pACC
tACC
FAS
SCD1
FADS2
GAPDH
Relative densitometry
pACC1
tACC1
p/tACC1
FAS
SCD1
FADS2
E
CON
CombAT
pACC
tACC
FAS
SCD1
FADS2
GAPDH
Relative densitometry
pACC1
tACC1
p/tACC1
FAS
SCD1
FADS2
F
Panc1
MiaPaCa2
Lipid amount
(pmol/ug total protein)
16:1n-7
16:1n-10
G
SCD activity
Panc1
MiaPaCa2
Normalised peak area
16:1n-7/16:0
H
FADS2 activity
Panc1
MiaPaCa2
Normalised peak area
16:1n-10/16:0
CON
CombAT
I
Chemo-naïve
Neoadj.
Normalised counts
ACACA
FASN
SCD
FADS2
J
Panc1
Relative growth
siNEG
siACACA
siFASN
siSCD
siFADS2
siSCD+siFADS2

327

328 **Figure 4:** Untargeted lipidomics of both **A** Panc1 and **B** MiaPaCa2 control (CON) and combination
329 therapy attenuated (CombAT) cell lines (unpaired t-test, $P < 0.01$). **C** *De novo* lipogenesis measured by
330 the incorporation of radiolabelled glucose into the lipid fraction. Immunoblotting for total and activated
331 key lipid synthesis enzymes in **D** Panc1 and **E** MiaPaC2 CON and CombAT cells. **F** 16:1 fatty acid
332 isomers measured by LC-MS of AMP^+-derivatised fatty acids. Measurement of **G** SCD1 and **H** FADS2
333 activity in Panc1 and MiaPaCa2 CON and CombAT cell lines by tracing uniformly stable-labelled
334 palmitic acid into isomeric MUFA. **I** Analysis of PDAC tumour RNAseq data published by Zhou and
335 colleagues obtained from patients who underwent surgical resection prior to chemotherapy (chemo-
336 naïve) or received GEMC/nab-paclitaxel neoadjuvant treatment (Neoadj.) before tumour resection. **J**
337 Effect of 72 h knockdown of lipid synthesis enzymes on Panc1 CombAT cell growth. Statistical
338 significance was determined by unpaired t test (**A-I**) or one-way ANOVA with Tukey posthoc
339 comparisons with *si*NEG only (**J**). *$P < 0.05$ ** $P < 0.01$. *** $P < 0.001$.

340 We next assessed if increased *de novo* lipogenesis persists in our CombAT cell lines, with both Panc1
341 and MiaPaCa2 CombAT cells demonstrating increased radiolabelled glucose incorporation into the
342 lipid fraction (Figure 4C). To better understand the specific metabolic pathways reprogrammed in
343 CombAT cells we performed immunoblotting of key lipid synthesis enzymes (Figure 4D&E). Panc1
344 CombAT cells had increases in both total and phosphorylated ACC1 (serine 79), leading to no change
345 in the ratio of phosphorylated to total ACC1 (Figure 4D). No changes were seen in FAS or SCD1 levels
346 between CombAT and CON Panc1 cells, while MiaPaCa2 CombAT cells had increased levels of
347 phosphorylated ACC1 and a small but statistically significant increase in SCD1 abundance (Figure 4E).

348 Combination chemotherapy resistance decreases FADS2 abundance and activity in 349 Panc1 cells

350 Surprisingly, FADS2 protein abundance was substantially decreased in Panc1 CombAT cells (Figure
351 4D). Similar to GEMR cell lines, little to no FADS2 protein was detected in MiaPaCa2 CombAT or
352 CON cells (Figure 4E) To confirm decreased FADS2 abundance in Panc1 CombAT cells we measured
353 FA 16:1 isomers in both cell lines by LC-MS/MS and found increased FA 16:1*n*-7 in Panc1 CombAT
354 cells alongside decreased FA 16:1*n*-10 (Figure 4F). Also observed in Panc1 CombAT were changes in
355 PUFA profile consistent with FADS2 downregulation, including decreases in FA 22:6*n*-3, FA 18:3*n*-6,
356 FA 20:4*n*-6, FA 22:4*n*-6 and FA 22:5*n*-6 when compared with CON (Figure S7). No changes were
357 detected in FA 16:1 isomeric profile in MiaPaCa2 CombAT cells when compared to CON (Figure 5F),
358 alongside no changes in PUFA levels (Figure S7C). To further confirm these findings, we measured
359 steady-state desaturase activity by tracing uniformly labelled ^{13}C-palmitate into both cell lines over 72
360 h. Neither cell line exhibited any differences between CON and CombAT cells in unlabelled FA 16:0
361 content (Figure S8A&B). However, Panc1 CombAT cells had more labelled palmitic acid (relative to
362 unlabelled palmitic acid) while MiaPaCa2 CombAT cells had less (Figure S8C&D respectively). No
363 differences were seen for SCD1 activity as measured by the ratio of labelled FA16:1*n*-7 to FA 16:0 in
364 Panc1 or MiaPaCa2 CombAT cells (Figure 4G). We also measured FADS2 activity in this cell line by
365 comparing labelled FA 16:1*n*-10 with its labelled FA 16:0 precursor, which confirmed a substantial
366 decrease in FADS2 activity in Panc1 CombAT cells (Figure 4H). No change in FA 16:1*n*-10/FA 16:0

367 was observed for MiaPaca2 CombAT cells. Also apparent in Panc1 CombAT cells was a marked
368 decrease in FAO compared with CON cells (Figure S9). Taken together, these data indicate that chronic
369 combination GEMC/PTX treatment strongly downregulates FADS2 abundance and activity in the
370 Panc1 cell line and decreases FAO. To explore if combination GEMC/PTX therapy might exhibit the
371 same effect on lipid metabolism in human PDAC patients, we analysed recently published RNA-seq
372 data obtained from PDAC patients who received no treatment (chemo-naïve) or GEMC/nab-paclitaxel
373 neoadjuvant chemotherapy prior to tumour resection (42). The data showed no difference in the
374 expression of *ACACA, FASN or SCD* between chemo-naïve or neoadjuvant-treated tumours; however,
375 the neoadjuvant group demonstrated a small but statistically significant decrease in *FADS2* expression
376 when compared with chemo-naïve tumours (Figure 4I). These data suggest that our *in vitro* findings of
377 combination chemotherapy downregulating FADS2 protein abundance potentially translate to human
378 PDAC patients treated with GEMC/PTX.

379 Given the effect of combination therapy resistance on FADS2 abundance and fatty acid isomer profile
380 we sought to understand if co-targeting both desaturases was still necessary to produce a decrease in
381 cell growth in Panc1 CombAT cell lines. Knockdown of *ACACA*, *FASN*, or *SCD* for 72 h in Panc1
382 CombAT cells resulted in a statistically significant decrease in cell growth when compared to negative
383 siRNA control (si*NEG*), with si*FASN* or si*SCD* producing the largest decreases in cell growth (Figure
384 5J). Consistent with the already decreased FADS2 levels, siRNA targeting *FADS2* in Panc1 CombAT
385 cells did not result in a change in cell growth, and simultaneous knockdown of both *SCD* and *FADS2*
386 did not produce a further decrease in growth above that of *SCD* alone. These data suggest that
387 therapeutically targeting SCD1 in combination with GEMC/PTX chemotherapy could be a viable
388 strategy for enhancing cytotoxicity in PDAC.

389 Discussion

390 We sought to characterise metabolic adaptations to chemotherapy exposure in PDAC and found
391 enhanced *de novo* lipogenesis in PDAC cells with resistance to both monotherapy GEMC and
392 combination GEMC/PTX chemotherapy. Enhanced *de novo* lipogenesis is a known feature of many
393 cancers, including pancreatic cancer (18), where increased expression of lipogenic genes is correlated
394 with poorer survival and greater resistance to chemotherapy (17). Herein we provide the first report of
395 enhanced *de novo* lipogenesis specifically in GEMC resistance in PDAC, providing a novel target for
396 the disease that could potentially improve treatment efficacy. We also provide the first report of
397 alternate saturated fatty acid desaturation in PDAC, whereby FA 16:0 is desaturated by FADS2 to
398 produce FA 16:1*n*-10. The ability of cancer cells to exhibit diversity in isomeric lipids has recently been
399 described in other cancer cell types including liver & lung cancer cell lines more extensively in prostate
400 cancer (35,37). This metabolic and isomeric diversity is proposed to promote metabolic plasticity

401 enabling cancer cells to survive and proliferate in challenging tumour microenvironments depleted in
402 bioenergetic fuels and oxygen.

403 In this work we specifically found upregulation of ACC1 (through increased total abundance or
404 decreased phosphorylation at Serine-79), FAS and SCD with GEMR. FAS is commonly expressed at
405 high levels in a variety of cancers of human tissues (23–25) and *FASN* overexpression correlates to
406 poorer survival and increased GEMC resistance in PDAC (17). High FAS levels have also been found
407 in the serum of patients with PDAC or intraductal papillary mucinous neoplasms (43). We found that
408 genetically inhibiting FAS (Panc1 & MiaPaCa2), SCD1 (MiaPaCa2) or SCD1 & FADS2 (Panc1) in
409 combination with GEMC produced the greatest impact on PDAC cell growth (Figure 4E). Previous
410 work demonstrated that inhibition of FAS by Orlistat induces ER stress and acts synergistically with
411 GEMC to decrease PDAC cell growth and reduce tumour burden in xenograft models of PDAC (17).
412 Orlistat has also been reported to attenuate oxaliplatin resistance in colorectal cancer (44). This
413 synergistic effect of Orlistat with chemotherapy *in vivo* may be related to a direct effect on FAS but
414 may also arise from the dual action of Orlistat on lipases that further inhibit the availability of free fatty
415 acids for use by cancer cells. However, Orlistat has poor bioavailability, is contraindicated in pancreatic
416 disease, and can cause pancreatitis in susceptible patients (45), all of which potentially limit its
417 therapeutic use in PDAC. Other small molecule inhibitors of FAS have had some success in decreasing
418 cancer cell growth *in vitro* and *in vivo*, including in breast, colon, lung, colorectal, bladder, ovarian,
419 gastric, endometrial, prostate, gastrointestinal cancers as well as in melanoma and lymphoma (reviewed
420 extensively by (23)). Cerulenin has previously been shown to re-sensitise cisplatin-resistant ovarian
421 cancer cell lines to treatment (46), while its more stable derivative C75 sensitises breast cancer cells to
422 cisplatin treatment (47). However, both cerulenin and C75 exhibit significant off-target and side effects
423 that preclude their clinical use (23). Newer FAS inhibitors TVB-3166 and fasnall show promise for
424 synergistically inhibiting cell viability when used in combination with tubuli*n*-stabilising drugs in
425 taxane-resistant prostate cancer (48). Mouse and human-derived mutant $KRAS^{G12D}$ lung cancer models
426 are sensitive to genetic or TVB-3664 inhibition of FAS (49). Moreover, high *FASN* and *SCD* expression
427 are correlated with mutant $KRAS^{G12D}$ in lung cancer (49), which could potentially explain the differences
428 between the two PDAC cell lines examined herein – Panc1 cells similarly contain $KRAS^{G12D}$ and GEMR
429 increased expression and activity of both lipogenic enzymes, while MiaPaCa2 cells contain $KRAS^{G12C}$.
430 In any event, targeting FAS could provide therapeutic benefits to PDAC patients when used in
431 combination with GEMC-based therapy; however, the development of a small molecule inhibitor with
432 good efficacy and a low side effect profile would be needed.

433 SCD1 has been described as an oncogene in lung cancer (50) and explored as a potential therapeutic
434 target for several cancers including PDAC (reviewed by (51)). SCD1 is highly expressed in the exocrine
435 pancreas (52) and, specifically in PDAC, increased expression of SCD1 in cancer-associated fibroblasts
436 correlates with decreased PDAC survival time and GEMC resistance (16). Higher levels of FA 16:1

437 and 18:1 are associated with aggressive subtypes of PDAC immortalised cells; however, positions of
438 unsaturation (*i.e.*, fatty acid isomers) were not determined in this previous work (31). Inhibition of
439 SCD1 using the small molecule inhibitor A939572 induces the unfolded protein response and decreases
440 the growth of pancreatic tumours in KPC mice and in $EPCAM^+$ organoids derived from KPC mouse
441 tumours (53). In this work, we also discovered significant MUFA desaturase products of FADS2 in the
442 Panc1 cell line as evidenced by the detection of unsaturation at the *n*-10 position in both FA 16:1 and
443 FA 18:1 fatty acid (Figure 2E). Alternative FADS2 activity has only recently been discovered in other
444 cancer cell types (35,37) but this is the first report specifically in pancreatic cancer. There is limited
445 exploration of FADS2 as a therapeutic target in cancer and existing data has largely focused on its role
446 in Δ6 desaturation of PUFA (54,55). FADS2 inhibition by small molecule inhibitor sc-26196 suppresses
447 prostaglandin E2 production via arachidonic acid and sensitises glioblastoma cells to radiotherapy in a
448 xenograft model (56). Genetic or pharmacological FADS2 inhibition also suppresses colon, lung,
449 melanoma, and cholangiocarcinoma cancer cell tumour growth in xenograft and genetically engineered
450 models (57–59). Pharmacologic or genetic dual-inhibition of SCD1 and FADS2 decreases tumour and
451 metastatic lesion growth and cancer stem cell formation in ovarian cancer while reducing resistance to
452 platinum-based chemotherapy (55). Our work and others (35,37) observed overcompensation by the
453 alternative desaturation pathway when SCD1 or FADS2 are individually inhibited in cancer cells
454 (Figure 4D). Indeed, this same compensatory desaturase effect might explain the observed decrease in
455 16:1*n*-10 and 18:1*n*-10 in Panc1 GEMR cells, where SCD1 abundance, activity, and MUFA products
456 were all increased when compared with Panc1 CON cells (Figure 2C, E, &F). Similarly, an increase in
457 *FADS2* expression has been observed when cells lines resistant to SCD1-inhibitors (A549 & HeLa) are
458 treated with A939572 (60). In our work, we show that there is suboptimal inhibition of PDAC cell
459 proliferation when only one desaturase is silenced alongside co-treatment with GEMC (Figure 4E).
460 Therefore, the use of SCD1 inhibitors might be sub-optimal in the presence of significant FADS2
461 abundance or activity; however, the extent of FADS2 protein abundance or activity in PDAC tumours
462 on a population level is not yet fully known.

463 This phenomenon of competing inhibitory pathways has previously been described and is thought to
464 enable enhanced plasticity at the expense of maximised proliferation (37,61,62). Such competing
465 pathways may also prove beneficial to cancer cell survival in PDAC as the hypoxic, nutrient-depleted
466 tumour microenvironment is particularly enhanced by the dense fibrosis associated with the disease
467 (63). Desaturation is a highly energy-demanding process, and desaturases are NADPH, O_2, and
468 cytochrome b5 dependent (64) - all of which are likely in short supply in the tumour microenvironment.
469 FADS2 contains a cytochrome b5-like domain meaning it is not wholly reliant on cytochrome b5 for
470 its activity, but FADS2 activity is enhanced in the presence of external cytochrome b5 (65). Specifically
471 in PDAC, mutant *KRAS* regulates GOT1 synthesis of NADPH from glutamine to maintain redox status
472 (66), but feasibly this pathway could also support high NADPH levels to maintain enhanced lipid

473 synthesis and desaturation. Though highly energy-demanding, desaturation would allow the
474 sequestration of highly lipotoxic SFA such as FA 16:0 and FA 18:0 into less toxic MUFA in lipogenic
475 cells, thus preventing cell death (67). Increased desaturation of lipids also modulates cell membrane
476 fluidity and is highly associated with epithelial-to-mesenchymal transition (EMT), a process crucial to
477 cell migration and metastatic initiation (68,69), and FADS2-derived FA 16:1*n*-10 specifically promotes
478 cell migration in melanoma cells (70). Expression of EMT transcription factor Zeb1 has been shown to
479 promote increased PUFA to MUFA ratio within cancer cells, with downregulation of Zeb1 suppressing
480 FADS2 and enhancing SCD1 & FAS expression (71). MUFA are also less susceptible to peroxidation
481 by reactive oxygen species (ROS) than PUFA, and given that ROS levels are often high in PDAC and
482 other cancers (72,73) increased MUFA would limit both ROS and cell death from iron-driven lipid
483 peroxidation (*i.e.* ferroptosis). Indeed, cells cultured with exogenous sources of MUFA have suppressed
484 ferroptosis (74) and SCD1 overexpression protects ovarian cancer cells from ferroptosis-mediated cell
485 death (75). Similarly, pharmacological inhibition of SCD1 sensitises cancer cells expressing high levels
486 of Zeb1 to ferroptosis (71). In short, despite the high energy demands associated with lipid desaturation
487 the process likely provides significant benefits for cancer cell survival that outweigh the energetic cost.

488 Our finding that combination GEMC/PTX resistance strongly downregulates FADS2 protein
489 abundance and activity in Panc1 cells was unexpected, as PTX has previously been shown to increase
490 FADS2 protein abundance in lung adenocarcinoma cells (76). The mechanism by which PTX combined
491 with GEMC downregulates FADS2 protein levels and activity is unknown, and FADS2 shares similar
492 transcriptional factors to ACC, FAS and SCD1 (77). Upregulated *FADS2* expression and increased
493 sapienic acid biosynthesis can be driven in multiple cancer cells lines by mammalian target of
494 rapamycin (mTOR) signalling and sterol regulatory element-binding protein (SREBP) (78); however,
495 little else is known about transcriptional or post-translational regulation of FADS2 abundance and
496 activity. Nevertheless, our results strongly suggest that combining SCD1 inhibition with GEMC/PTX
497 chemotherapy could be an effective strategy for decreasing PDAC cell growth without the need to
498 include a FADS2 inhibitor where desaturase diversification is apparent. This could be important for
499 accelerated translational efforts as a therapeutic target as only a single small molecule inhibitor is
500 currently available for FADS2 (sc-26196), and its *in vivo* safety and efficacy profile is yet to be
501 established in humans. Importantly PDAC patients who received GEMC/PTX neoadjuvant treatment
502 show decreased *FADS2* expression (Figure 5I), further highlighting the potential translatability of our
503 findings.

504 In summary, we have identified that *de novo* lipogenesis is increased in GEMC-resistant PDAC cells
505 including the presence of an alternate desaturation pathway in Panc1 cells. We identify several key lipid
506 metabolic pathways including ACC1, FAS, SCD1 and FADS2 that could be targeted to improve GEMC
507 efficacy on cell growth. Importantly, we have determined that SCD1 and FADS2 can compensate for
508 each other in PDAC, and that where dual desaturase activity exists both desaturases must be targeted to

509 provide the best effect. Finally, we provide evidence that combination GEMC/PTX therapy strongly
510 downregulates FADS2 expression and activity and increases the efficacy of SCD1 inhibition in PDAC
511 cells with dual desaturase activity. Therefore, we conclude that co-targeting lipid synthesis in PDAC
512 could be a viable strategy for improving the efficacy of both GEMC monotherapy and combination
513 GEMC/PTX therapy in patients.

514 Method details

515 Materials

516 Gemcitabine hydrochloride, paclitaxel and foetal calf serum (FCS) were purchased from BioStrategy
517 (Melbourne, VIC, Australia). High glucose DMEM was purchased from ThermoFisher Scientific
518 (Melbourne, VIC, Australia). All solvents and additives used for liquid chromatography-mass
519 spectrometry (LC-MS) were HPLC grade or higher and were purchased from ThermoFisher Scientific.
520 Crystal violet and LC-MS grade water were purchased from Merck Life Sciences (Melbourne, VIC,
521 Australia). All lipid internal standards were purchased from Merck Life Sciences except diacylglycerol
522 15:0/15:0 (Nu-Chek Prep, Elysian, MN, USA) and d5-triacylglycerol 16:0/16:0/16:0 (C/D/N Isotopes,
523 Quebec, Canada). Antibodies for immunoblotting were purchased from Cell Signaling Technology
524 (Danvers, MA, USA), Abclonal (Woburn, MA, USA) Abcam (Melbourne, VIC, Australia), or Santa
525 Cruz Biotechnology (Dallas, TX, USA) as indicated in Table S1. MUFA isomer standards were
526 purchased from Sapphire Bioscience (Sydney, NSW, Australia).

527 Cell culture & chemotherapy resistance generation

528 Panc1 and MiaPaCa2 cells from ATCC were cultured in high glucose Dulbecco's Modified (DMEM)
529 containing 4.5 g/L glucose and were supplemented with 10% FCS. Cells were cultured under 5% CO_2
530 at 37ºC and routinely passaged every 2-3 days (when ~80-90% confluent). GEMC resistance was
531 induced in PDAC cell lines through increasing doses over 10-12 weeks. Each cell line was treated with
532 the highest tolerable dose of gemcitabine for 48 h and allowed to recover until normal proliferation was
533 observed (1-3 weeks). This process was repeated a minimum of three times before comparing the half-
534 maximal inhibitory concentration (IC_{50}) with untreated cells of the same PDAC line. If the IC_{50} in the
535 GEMC-treated group was higher than CON then resistance was determined to have been established. If
536 not, then the concentration of GEMC was increased, and the process repeated. CombAT cells were
537 generated similarly through repeat escalating doses of GEMC/PTX (10:1 v/v) for 12 weeks.

538 Measurement of half-maximal inhibitory concentration

539 The IC_{50} was determined using a crystal violet assay. Cells were seeded at 1×10^4 cells/well into a 96-
540 well plate in triplicate and allowed to adhere overnight. The next day cells were treated with serial
541 dilutions of GEMC (phosphate buffered saline, PBS, as vehicle) or GEMC:PTX (10:1, with PBS+0.1%
542 ethanol as the vehicle). The IC_{50} was measured after 48 h by crystal violet assay. Briefly, media was

543 removed from adherent cells and cells were washed once with PBS. Cells were fixed in a solution of
544 0.5% w/v crystal violet in 50% v/v methanol for a minimum of 10 min. After fixation, cells were washed
545 with water to remove excess crystal violet and allowed to dry overnight. Stained adherent cells were
546 then solubilised in 1% w/v SDS by vigorous shaking for several hours following which the absorbance
547 was read at 570 nm. Absorbance values were normalised to the vehicle and the IC_{50} was calculated by
548 a non-linear regression by fitting the $\log_{10}$ transformed drug concentration against relative cell viability.
549 Statistical significance was determined by comparing a four-parameter curve fit using the extra sum of
550 squares F test ($P < 0.05$).

551 **BODIPY staining and confocal imaging**

552 For BODIPY staining and confocal imaging, cells were seeded in a 96 well plate at 10,000 cells/well
553 and allowed to grow to near-confluency. Cells were then fixed with 4% paraformaldehyde (PFA) for
554 10 min at room temperature, followed by PBS washes. Permeabilization was performed for 10 min
555 using a saponin-based permeabilization/blocking buffer (0.2% (w/v) saponin, 4% (v/v) FBS, 1% (w/v)
556 BSA, and 0.02% (v/v) sodium azide in PBS). Next, cells were incubated for 2 h with Alexa Fluor® 647
557 anti-Tubulin-α antibody (1:250 dilution, clone 10D8, BioLegend) prepared in the
558 permeabilization/blocking buffer. After several washes with PBS, 200 nM BODIPY 493/503 (Cat. No.
559 25892, Cayman Chemical) and Hoechst 33342 (10 µg/mL, B2261-25MG, Sigma-Aldrich) were added
560 in permeabilization buffer for 10 min at room temperature, followed by PBS washes. Confocal images
561 were acquired using an LSM900 confocal laser scanning microscope with a 40x objective. Lipid
562 droplets per cell and droplet size were quantified using Fiji software.

563 **Lipid extraction**

564 Lipids were extracted from cells grown to 80-90% confluency in 6 well plates using a modified methyl
565 *tert*-butyl ether (MTBE) method (79,80). Adherent cells were washed with ice-cold PBS and scraped
566 into methanol containing 0.01% butylated hydroxytoluene and 100 pmol of internal standards
567 (phosphatidylcholine 19:0/19:0, phosphatidylethanolamine 17:0/17:0, phosphatidylserine 17:0/17:0,
568 lysophosphatidylcholine 17:0, lysophosphatidylethanolamine 14:0, phosphatidylglycerol 17:0/17:0,
569 phosphatidic acid 17:0/17:0, ceramide d18:1/17:0, dihydrosphingomyelin 12:0, cholesteryl ester 22:1,
570 diacylglycerol 17:0/17:0, D_5-triacylglycerol 16:0/16:0/16:0 and cardiolipin 14:0/14:0/14:0/14:0). An
571 empty well was also scraped for use in background subtraction. To this, MTBE was added at a ratio of
572 3:1 v/v, and extracts were rotated overnight at 4ºC. Following overnight rotation, 1 part of ice-cold 150
573 mM ammonium acetate was added, samples were vortexed vigorously and centrifuged at 2000 *x g* for
574 5 min. The upper organic phase containing lipids was transferred into a 1.5 mL autosampler vial and
575 dried under N_2 at 37ºC Dried lipids were reconstituted in chloroform:methanol:water (60:30:4.5 v/v/v),
576 transferred to a sleeved vial, and stored at -20ºC until analysis. The aqueous phase containing the protein
577 pellet was dried under N_2 and digested with 1M NaOH overnight at 4ºC. Digested protein was diluted

578 1:2 v/v with water and protein concentration was determined using a Pierce BCA assay kit
579 (ThermoFisher Scientific)

580 **Untargeted lipidomics**

581 Untargeted lipidomics was performed as previously described (81). Untargeted lipidomics was
582 performed by liquid chromatography-mass spectrometry (LC-MS) using a Dionex Ultimate 3000 LC
583 pump and Q Exactive Plus mass spectrometer equipped with a heated electrospray ionization (HESI)
584 source (ThermoFisher Scientific, Waltham, MA, USA) (82–84). Lipids were separated on a core-shell
585 hybrid C18 reverse-phase column (ACQUITY C18 CSH, 2.1 x 100 mm, 1.7µm pore size, Waters Corp.,
586 Milford, MA) using a binary gradient, where mobile phase A consisted of acetonitrile:water (6:4 v/v)
587 and B of isopropanol: acetonitrile (9:1 v/v). Both mobile phases A and B contained 10 mM ammonium
588 formate and 0.1% formic acid. The autosampler was kept chilled at 10ºC, the column was heated to
589 60ºC, and the flow rate was maintained at 0.26 ml/min throughout. Source conditions were as follows:
590 a spray voltage 4.0 kV in positive ion mode and 3.5 kV in negative ion mode, capillary temperature
591 290°C, S lens RF 50, and auxiliary gas heater temperature of 250°C. Nitrogen was used as both source
592 and collision gas, with the sheath gas flow rate set at 20 and the auxiliary gas flow rate at 5 (arbitrary
593 units). Data were acquired in full scan/data-dependent MS2 mode (full-scan resolution 70,000 FWHM,
594 max ion injection time 50 ms, scan range m/z 200–1,500), with the 10 most abundant ions being
595 subjected to collision-induced dissociation using an isolation window of 1.5 Da and a normalized
596 stepped collision energy of 15/27 eV. Product ions were detected at a resolution of 17,500. An exclusion
597 list for background ions was developed using extraction blanks, and mass calibration was performed in
598 both positive and negative ionization modes before analysis to ensure mass accuracy of 5 ppm in full-
599 scan mode.

600 Lipids were identified using MS-DIAL v4.9 (85). Lipids were detected in both positive and negative
601 ionization modes using a minimum peak height of $1x10^4$ cps, an MS1 tolerance of 5 ppm and MS2
602 tolerance of 10 ppm, and a minimum identification score of 50%. Identified peaks were aligned with a
603 retention time (RT) tolerance of 0.5 min. Exported aligned data were background subtracted, quantified
604 from internal standards, and normalised to protein using the statistical package R.

605 ***De novo* lipogenesis assay using [U-14]C labelled glucose**

606 Cells were seeded in 6 well plates and allowed to grow to near-confluence (80-90%, ~$1\text{-}2\times10^6$
607 cells/well). Briefly, cells were washed with PBS and incubated in DMEM containing 1 g/L D-glucose
608 and 2 µCi/mL [U-14C]C-glucose (Perkin Elmer, Sydney, NSW, Australia) for 2 h at 37°C. Following
609 this, cells were washed and scraped into ice-cold PBS. Cells were lysed by passing repeated through a
610 fine gauge needle, and an aliquot was taken for protein determination by BCA assay. Lipids were
611 extracted from the remaining sample by Folch extraction (86). The lower lipid-containing organic phase

612 was removed to a new vial and dried under N_2 at 37ºC before being reconstituted in scintillation fluid
613 (Ultima Gold, Perkin Elmer, Sydney, NSW, Australia). ^{14}C content was determined by direct DPM
614 assay using a beta counter (TriCarb liquid scintillation counter, Perkin Elmer) and normalised to total
615 protein.

616 **Western blotting**

617 For immunoblotting of lipid synthesis enzymes cells were grown to near-confluency on 6 well plates
618 (~1-2×10^6 cells/well). Cells were washed with ice-cold PBS and scraped into ice-cold
619 radioimmunoprecipitation assay (RIPA) buffer containing protease and phosphatase inhibitors (10
620 µg/mL phenylmethylsulfonyl fluoride, 10 µg/mL aprotinin, 10 µg/mL leupeptin, 1 mM Na_3VO_4, and
621 10 mM NaF). Cells were lysed by repeated freeze/thawing on ice using liquid N_2, before being
622 centrifuged at 16,100 *x g* (4ºC) for 5 min. The lysate supernatant was removed to a new vial, from which
623 the protein concentration was determined by BCA assay. Lysates were resuspended in laemelli buffer,
624 and 10-15 ug of protein was separated by SDS polyacrylamide gel electrophoresis (10%). Proteins were
625 transferred onto 0.2 µm polyvinylidene fluoride membrane and protein bands visualised by Ponceau S
626 staining. Destained membranes were blocked in 5% w/v skim milk in Tris-buffered saline containing
627 0.1% Tween20 (TBST) for 1 h, before being incubated in primary antibody (1:1000) overnight (Table
628 S1). Membranes were washed with TBST before being incubated with an appropriate secondary
629 antibody conjugated to horse radish peroxidase (1:10,000, 5% w/v skim milk in TBST) for 1 h.
630 Membranes were washed in TBST and antibodies were detected by enhanced chemiluminescence
631 (Clarity Western ECL substrate, Bio-Rad Laboratories, Sydney NSW, Australia, or SuperSignal West
632 Femto Maximum Sensitivity Substrate, ThermoFisher Scientific) and imaged using a ChemiDoc
633 imaging system (Bio-Rad Laboratories). Densitometry was performed using Image Lab v6.1 (Bio-Rad
634 Laboratories) and normalised to the mean of the control group.

635 **Hydrolysis and AMP derivatisation of fatty acids**

636 Lipids were extracted from adherent cells grown to near-confluency in 6 well plates using the procedure
637 described above with the addition of 20 nmol of methyl nonadecanoate (Merck Life Science) as an
638 internal standard. Following MTBE extraction of lipids, an aliquot was taken and hydrolysed in 0.6 M
639 KOH in 75% v/v methanol at 60ºC for 30 min. Samples were then cooled to room temperature and
640 neutralised with 25% v/v acetic acid. Water and *n*-hexane (3:2 v/v) were added separately and samples
641 were vortexed vigorously before being centrifuged at 2000 *x g* for 5 min. The upper phase containing
642 hydrolysed fatty acids was removed, and the aqueous phase was washed with a second volume of *n*-
643 hexane and combined. The combined organic phase was then dried under N_2 at 37°C. Dried hydrolysed
644 fatty acids were derivatised with an AMP+ MaxSpec kit (Cayman Chemical, Ann Arbor, MI, USA) as
645 per manufacturer instructions (87). Following this, AMP-derivatised fatty acids were re-extracted using
646 MTBE:water (1:1 v/v), and the upper MTBE phase was dried under N_2 before being resuspended in

647 methanol. Samples were stored at -20°C until analysis. A 37-component fatty acid methyl ester standard
648 (Merck Life Sciences) containing an additional 3.184 nmol of methyl nonadecanoate was concurrently
649 subjected to the same derivatisation procedure and used as an external quality control for fatty acid
650 identification by LC-MS. Derivatised MUFA standards FA 16:1*n*-9,*cis*, FA 16:1*n*-10,*cis*, FA 18:1*n*-
651 7,*cis*, FA 18:1*n*-10,*cis*, and FA 18:1*n*-12,*cis* were also spiked into this mixture to generate retention
652 times (RT) for MUFA isomer identification by LC-MS.

653 **OzFAD analysis of AMP-derivatised fatty acids**

654 Ozone-enabled fatty acid discovery analysis was conducted as previously described (38). Briefly, 10
655 µL injections of AMP+ derivatized fatty acids were subjected to reversed-phase chromatography using
656 a Waters ACQUITY Class UPLC (Waters Corporation, Milford, USA) fitted with an ACQUITY C18
657 reversed-phase column (2.1 × 100 mm i.d., particle size 1.7 µm, Waters Corporation) maintained at 60
658 °C. The 20 min gradient utilised a binary mobile phase system comprised A: water (0.1% formic acid)
659 and B: acetonitrile (0.1% formic acid). Chromatographic detection was conducted using an ion-mobility
660 enabled quadrupole time of flight (QTOF) mass spectrometer (SYNAPT G2-S*i* HDMS, Waters
661 Corporation) previously modified to allow introduction of high concentration ozone into the ion
662 mobility region of the instrument (88). Electrospray ionisation parameters were: capillary +3 kV,
663 sampling cone +40 V, source temperature 120 °C, desolvation temperature 550 °C, cone gas 100 L/h,
664 desolvation gas 900 L/h, and nebulizer gas pressure 6.5 bar. Gas flows to the ion mobility region of the
665 instrument were 2.0, 180 and 90 mL/min, for the trap, helium cell and IMS region, respectively. For the
666 ozonolysis reactions, oxygen (≥ 99.999%, Coregas, NSW, Australia) was converted to ozone at
667 concentrations of 220-240 g/Nm^3 (~15-17% O_3 in O_2) using a high concentration ozone generator (TG-
668 40, Ozone Solutions, Hull, IA). Peak areas for Criegee and aldehyde ions for each monounsaturated
669 fatty acid isomer were combined and normalised to internal standard and total protein (measured by
670 BCA assay).

671 **Desaturase activity determination**

672 Cells were seeded in 6 well plates at a density of 3×10^5 cells/well and allowed to adhere overnight. The
673 following day, cell culture media was changed to FCS-free high glucose DMEM containing 12.5 µM
674 $^{13}C_{16}$-labelled or unlabelled palmitate conjugated to 2% fatty acid-free bovine serum albumin (BSA,
675 Merck Life Sciences). Palmitate was prepared in cell culture media from 100 mM ethanolic stocks of
676 palmitic acid and conjugated to fatty acid-free BSA by incubating at 55°C in media for 2 h. Lipids were
677 extracted and derivatised as described above after 72 h of incubation with labelled or unlabelled
678 palmitate Lipids were identified and analysed as described below for LC-MS analysis of AMP-
679 derivatised fatty acids, with labelled fatty acids identified from $[M+H+16.0542]^+$ precursors with the
680 same RT as their unlabelled counterparts as per Table S2.

681 **LC-MS analysis of AMP-derivatised fatty acids**

682 AMP-derivatised fatty acids were separated on a core-shell C30 reverse phase column (Accucore 2.6
683 µm, 2.1 x 150 mm, ThermoFisher Scientific) on an Agilent 1290 Infinity II HPLC pump (Agilent
684 Technologies Inc, Santa Clara, CA, USA) using a modified gradient to that described above for OzFAD
685 analysis. Mobile phase A consisted of water and mobile phase B of acetonitrile (both containing 0.1%
686 formic acid), the flow rate was set at 0.4 mL/min throughout and the column heater at 30°C. The
687 gradient was as follows: 0-3.25 min increase from 50% B to 56% B, 3.25-6.5 min increase to 58% B,
688 6.5-7.5 min increase to 80% B, 7.5-9.5 min increase to 100% B, hold at 100% B for 1.5 mins. The
689 column was then re-equilibrated at 50% B for 4.5 mins. AMP-derivatised fatty acids were detected as
690 positive ions in QTOF-only mode on an Agilent 6560 IM-MS QTOF mass spectrometer (Agilent
691 Technologies). Source conditions were as follows: capillary voltage of 3.5 kV, nozzle voltage of 1 kV
692 and fragmentor at 360 V. Nitrogen was used as the sheath and collision gas, with drying gas set at 5
693 L/min and sheath gas at 12 L/min (both gases heated to 300°C) and the nebuliser pressure set at 20 psi.
694 Ions were acquired in Auto MS/MS mode at an MS1 mass range of *m/z* 100-1000 and MS2 mass range
695 of *m/z* 50-600. Spectra were acquired in MS1 mode at 5 spectra/s and 200 ms/spectrum, and in MS2
696 mode at 10 spectra/s and 100 ms/spectrum. Precursor ions were isolated using a window of 1.3 Th,
697 acquisition time of 50 ms/spectra, and collision energy of 45 eV. Calibration mix A was infused
698 throughout and masses were automatically detected and corrected using a 100 ppm window and
699 minimum height of 1×10^3 counts to ensure 5 ppm mass accuracy, with *m/z* 121.050873 and 922.009798
700 used as reference ions. AMP-derivatised fatty acids as $[M+H]^+$ were aligned using Mass Profinder v10.0
701 (Agilent Technologies) with an RT tolerance of 0.5 min and MS1 tolerance of 10 ppm. Lipids were
702 identified using a custom personal compound database and library (PCDL) generated from the RT of
703 external quality control samples (Table S2) and MS/MS spectra were manually inspected to ensure
704 correct MUFA isomer identification. Using this method, FA 18:1 isomers were only partially separated
705 and so these data were not analysed further. Data were exported, blank subtracted and quantified from
706 internal standards before being normalised to total protein.

707 **Knockdown by small interfering RNA**

708 Knockdown experiments were performed in adherent cells grown in 6 well plates for 72 h. Cells were
709 seeded at $1\text{-}3\times10^5$ cells/well and allowed to adhere overnight. Cells were transfected with Silencer
710 Select siRNA targeting *ACACA* (s883), *FASN* (s5030), *SCD* (s12505,s12504) *FADS2* (s18025,s18023)
711 or negative control (Silencer Select Negative Control No. 1) using Lipofectamine RNAiMAX
712 transfection reagent as per the manufacturer's instructions (ThermoFisher Scientific).

713 **RNAseq dataset analysis**

714 PDAC tumour RNAseq data previously published by Zhou et al. (42) were used in this analysis. Genes
715 of interest (*ACACA*, *FASN*, *SCD*, *FADS2*) were filtered from the main dataset, alongside patients who
716 received either neo-adjuvant (Neoadj, n=9) or adjuvant (chemo-naïve, n=66) gemcitabine/nab-
717 paclitaxel treatment. Normalised counts were compared between the groups by unpaired t text ($p <$
718 0.05).

719 **Statistical analysis**

720 Unless otherwise stated, all data were analysed by comparing CON with GEMR or CombAT cell lines
721 using an unpaired t-test with statistical significance set at $P < 0.05$. Data are expressed as means ±
722 standard error of the mean (SEM).

723 **Acknowledgements**

724 The authors acknowledge the use of the UNSW Sydney Mark Wainwright Bioanalytical Mass
725 Spectrometry Facility, QUT Central Analytical Research Facility, and Victor Chang Cardiac Research
726 Institute Innovation Centre Metabolomics & Microimaging Facilities (funded by the New South Wales
727 Government Ministry of Health) in this work.

728 **Funding sources**

729 This project was supported by a Young Investigator Priority-driven Collaborative Cancer Research
730 Grant (APP1160909, funded by Cure Cancer Australia and Can Too!) awarded to SEH, a Miltenyi
731 Research Award (2022) & Victor Chang Cardiac Research Institute Outstanding Early and Mid-career
732 Researcher Grant award to OC, and a PanKind Accelerator grant awarded to NT, SEH, and SJB. BLJP
733 and SJB acknowledge support for enabling technologies from the Australian Research Council
734 Discovery (DP190101486) and Linkage Project (LP180100238).

735

736

737

References

1. Sung H, Ferlay J, Siegel RL, Laversanne M, Soerjomataram I, Jemal A, et al. Global Cancer Statistics 2020: GLOBOCAN Estimates of Incidence and Mortality Worldwide for 36 Cancers in 185 Countries. CA Cancer J Clin. 2021;71(3):209–49.

2. Rawla P, Sunkara T, Gaduputi V. Epidemiology of Pancreatic Cancer: Global Trends, Etiology and Risk Factors. World J Oncol. 2019 Feb;10(1):10–27.

3. Kleeff J, Korc M, Apte M, La Vecchia C, Johnson CD, Biankin AV, et al. Pancreatic cancer. Nat Rev Dis Primer. 2016 Apr 21;2(1):1–22.

4. Conroy T, Desseigne F, Ychou M, Bouché O, Guimbaud R, Bécouarn Y, et al. FOLFIRINOX versus Gemcitabine for Metastatic Pancreatic Cancer. N Engl J Med. 2011 May 12;364(19):1817–25.

5. Chun JW, Lee SH, Kim JS, Park N, Huh G, Cho IR, et al. Comparison between FOLFIRINOX and gemcitabine plus nab-paclitaxel including sequential treatment for metastatic pancreatic cancer: a propensity score matching approach. BMC Cancer. 2021 May 11;21(1):537.

6. Tempero MA, Pelzer U, O'Reilly EM, Winter J, Oh DY, Li CP, et al. Adjuvant nab-Paclitaxel + Gemcitabine in Resected Pancreatic Ductal Adenocarcinoma: Results From a Randomized, Open-Label, Phase III Trial. J Clin Oncol Off J Am Soc Clin Oncol. 2022 Dec 15;JCO2201134.

7. Bailey P, Chang DK, Nones K, Johns AL, Patch AM, Gingras MC, et al. Genomic analyses identify molecular subtypes of pancreatic cancer. Nature. 2016 Mar;531(7592):47–52.

8. Jones S, Zhang X, Parsons DW, Lin JCH, Leary RJ, Angenendt P, et al. Core signaling pathways in human pancreatic cancers revealed by global genomic analyses. Science. 2008 Sep 26;321(5897):1801–6.

9. Hezel AF, Kimmelman AC, Stanger BZ, Bardeesy N, DePinho RA. Genetics and biology of pancreatic ductal adenocarcinoma. Genes Dev. 2006 May 15;20(10):1218–49.

10. Liu YH, Hu CM, Hsu YS, Lee WH. Interplays of glucose metabolism and KRAS mutation in pancreatic ductal adenocarcinoma. Cell Death Dis. 2022 Sep 24;13(9):1–10.

11. Yao W, Maitra A, Ying H. Recent insights into the biology of pancreatic cancer. EBioMedicine. 2020 Mar 1;53:102655.

12. Myo Min KK, Ffrench CB, Jessup CF, Shepherdson M, Barreto SG, Bonder CS. Overcoming the Fibrotic Fortress in Pancreatic Ductal Adenocarcinoma: Challenges and Opportunities. Cancers. 2023 Apr 18;15(8):2354.

13. Hardie RA, van Dam E, Cowley M, Han TL, Balaban S, Pajic M, et al. Mitochondrial mutations and metabolic adaptation in pancreatic cancer. Cancer Metab. 2017 Jan 30;5:2.

14. Gatto F, Schulze A, Nielsen J. Systematic Analysis Reveals that Cancer Mutations Converge on Deregulated Metabolism of Arachidonate and Xenobiotics. Cell Rep. 2016 Jul 19;16(3):878–95.

15. Kaoutari AE, Fraunhoffer NA, Hoare O, Teyssedou C, Soubeyran P, Gayet O, et al. Metabolomic profiling of pancreatic adenocarcinoma reveals key features driving clinical outcome and drug resistance. EBioMedicine. 2021 Apr 1;66:103332.

16. Wu C, Hu B, Wang L, Wu X, Gu H, Dong H, et al. Assessment of stromal SCD-induced drug resistance of PDAC using 3D-printed zPDX model chips. iScience. 2022 Dec 5;26(1):105723.

17. Tadros S, Shukla SK, King RJ, Gunda V, Vernucci E, Abrego J, et al. De Novo Lipid Synthesis Facilitates Gemcitabine Resistance through Endoplasmic Reticulum Stress in Pancreatic Cancer. Cancer Res. 2017 Oct 15;77(20):5503–17.

18. Sunami Y, Rebelo A, Kleeff J. Lipid Metabolism and Lipid Droplets in Pancreatic Cancer and Stellate Cells. Cancers. 2017 Dec 23;10(1):3.

19. Rozeveld CN, Johnson KM, Zhang L, Razidlo GL. KRAS Controls Pancreatic Cancer Cell Lipid Metabolism and Invasive Potential through the Lipase HSL. Cancer Res. 2020 Nov 13;80(22):4932–45.

20. Wang G, Yao H, Gong Y, Lu Z, Pang R, Li Y, et al. Metabolic detection and systems analyses of pancreatic ductal adenocarcinoma through machine learning, lipidomics, and multi-omics. Sci Adv. 2021 Dec 22;7(52):eabh2724.

21. Auciello FR, Bulusu V, Oon C, Tait-Mulder J, Berry M, Bhattacharyya S, et al. A Stromal Lysolipid–Autotaxin Signaling Axis Promotes Pancreatic Tumor Progression. Cancer Discov. 2019 May 1;9(5):617–27.

22. Broadfield LA, Pane AA, Talebi A, Swinnen JV, Fendt SM. Lipid metabolism in cancer: New perspectives and emerging mechanisms. Dev Cell. 2021 May 17;56(10):1363–93.

23. Fhu CW, Ali A. Fatty Acid Synthase: An Emerging Target in Cancer. Molecules. 2020 Aug 28;25(17):3935.

24. Kuhajda FP. Fatty-acid synthase and human cancer: new perspectives on its role in tumor biology. Nutrition. 2000 Mar 1;16(3):202–8.

25. Vanauberg D, Schulz C, Lefebvre T. Involvement of the pro-oncogenic enzyme fatty acid synthase in the hallmarks of cancer: a promising target in anti-cancer therapies. Oncogenesis. 2023 Mar 18;12(1):1–10.

26. Yuan Y, Yang X, Li Y, Liu Q, Wu F, Qu H, et al. Expression and prognostic significance of fatty acid synthase in clear cell renal cell carcinoma. Pathol - Res Pract. 2020 Nov 1;216(11):153227.

27. Yang Y, Li H, Li Z, Zhao Z, Yip-Schneider M, Fan Q, et al. Role of fatty acid synthase in gemcitabine and radiation resistance of pancreatic cancers. Int J Biochem Mol Biol. 2011 Jan 31;2(1):89–98.

28. Ghaeidamini Harouni M, Rahgozar S, Rahimi Babasheikhali S, Safavi A, Ghodousi ES. Fatty acid synthase, a novel poor prognostic factor for acute lymphoblastic leukemia which can be targeted by ginger extract. Sci Rep. 2020 Aug 21;10(1):14072.

29. Liu H, Wu X, Dong Z, Luo Z, Zhao Z, Xu Y, et al. Fatty acid synthase causes drug resistance by inhibiting TNF-α and ceramide production[S]. J Lipid Res. 2013 Mar 1;54(3):776–85.

30. Suzuki T, Otsuka M, Seimiya T, Iwata T, Kishikawa T, Koike K. The biological role of metabolic reprogramming in pancreatic cancer. MedComm. 2020 Nov 5;1(3):302–10.

31. Daemen A, Peterson D, Sahu N, McCord R, Du X, Liu B, et al. Metabolite profiling stratifies pancreatic ductal adenocarcinomas into subtypes with distinct sensitivities to metabolic inhibitors. Proc Natl Acad Sci. 2015 Aug 11;112(32):E4410–7.

816 32. Chen C, Zhao S, Zhao X, Cao L, Karnad A, Kumar AP, et al. Gemcitabine resistance of pancreatic
817 cancer cells is mediated by IGF1R dependent upregulation of CD44 expression and isoform
818 switching. Cell Death Dis. 2022 Aug 5;13(8):1–13.

819 33. El Amrani M, Corfiotti F, Corvaisier M, Vasseur R, Fulbert M, Skrzypczyk C, et al. Gemcitabine-
820 induced epithelial-mesenchymal transition-like changes sustain chemoresistance of pancreatic
821 cancer cells of mesenchymal-like phenotype. Mol Carcinog. 2019;58(11):1985–97.

822 34. Wang R, Cheng L, Xia J, Wang Z, Wu Q, Wang Z. Gemcitabine resistance is associated with
823 epithelial-mesenchymal transition and induction of HIF-1α in pancreatic cancer cells. Curr Cancer
824 Drug Targets. 2014;14(4):407–17.

825 35. Young RSE, Bowman AP, Williams ED, Tousignant KD, Bidgood CL, Narreddula VR, et al.
826 Apocryphal FADS2 activity promotes fatty acid diversification in cancer. Cell Rep [Internet]. 2021
827 Feb 9 [cited 2021 Feb 16];34(6). Available from: https://www.cell.com/cell-
828 reports/abstract/S2211-1247(21)00051-6

829 36. Guillou H, Zadravec D, Martin PGP, Jacobsson A. The key roles of elongases and desaturases in
830 mammalian fatty acid metabolism: Insights from transgenic mice. Prog Lipid Res. 2010
831 Apr;49(2):186–99.

832 37. Vriens K, Christen S, Parik S, Broekaert D, Yoshinaga K, Talebi A, et al. Evidence for an
833 alternative fatty acid desaturation pathway increasing cancer plasticity. Nature. 2019 Feb 6;1.

834 38. Menzel JP, Young RSE, Benfield AH, Scott JS, Wongsomboon P, Cudlman L, et al. Ozone-enabled
835 fatty acid discovery reveals unexpected diversity in the human lipidome. Nat Commun. 2023 Jul
836 4;14(1):3940.

837 39. Garajová I, Peroni M, Gelsomino F, Leonardi F. A Simple Overview of Pancreatic Cancer
838 Treatment for Clinical Oncologists. Curr Oncol. 2023 Oct 31;30(11):9587–601.

839 40. Ueno H, Ikeda M, Ueno M, Mizuno N, Ioka T, Omuro Y, et al. Phase I/II study of nab-paclitaxel
840 plus gemcitabine for chemotherapy-naive Japanese patients with metastatic pancreatic cancer.
841 Cancer Chemother Pharmacol. 2016 Mar 1;77(3):595–603.

842 41. Von Hoff DD, Ervin T, Arena FP, Chiorean EG, Infante J, Moore M, et al. Increased Survival in
843 Pancreatic Cancer with nab-Paclitaxel plus Gemcitabine. N Engl J Med. 2013 Oct
844 31;369(18):1691–703.

845 42. Zhou X, An J, Kurilov R, Brors B, Hu K, Peccerella T, et al. Persister cell phenotypes contribute
846 to poor patient outcomes after neoadjuvant chemotherapy in PDAC. Nat Cancer. 2023
847 Sep;4(9):1362–81.

848 43. Walter K, Hong SM, Nyhan S, Canto M, Fedarko N, Klein A, et al. Serum Fatty Acid Synthase as
849 a Marker of Pancreatic Neoplasia. Cancer Epidemiol Biomarkers Prev. 2009 Sep 10;18(9):2380–
850 5.

851 44. Han L, Dai W, Luo W, Ye L, Fang H, Mo S, et al. Enhanced De Novo Lipid Synthesis Mediated
852 by FASN Induces Chemoresistance in Colorectal Cancer. Cancers. 2023 Jan;15(3):562.

853 45. Ahmad FA, Mahmud S. Acute Pancreatitis Following Orlistat Therapy: Report of Two Cases. J
854 Pancreas. 11(1):0–0.

855 46. Bauerschlag DO, Maass N, Leonhardt P, Verburg FA, Pecks U, Zeppernick F, et al. Fatty acid
856 synthase overexpression: target for therapy and reversal of chemoresistance in ovarian cancer. J
857 Transl Med. 2015 May 7;13:146.

858 47. Al-Bahlani S, Al-Lawati H, Al-Adawi M, Al-Abri N, Al-Dhahli B, Al-Adawi K. Fatty acid
859 synthase regulates the chemosensitivity of breast cancer cells to cisplatin-induced apoptosis.
860 Apoptosis. 2017 Jun 1;22(6):865–76.

861 48. Souchek JJ, Laliwala A, Houser L, Muraskin L, Vu Q, Mohs AM. Fatty Acid Synthase Inhibitors
862 Enhance Microtubule-Stabilizing and Microtubule-Destabilizing Drugs in Taxane-Resistant
863 Prostate Cancer Cells. ACS Pharmacol Transl Sci. 2023 Dec 8;6(12):1859–69.

864 49. Bartolacci C, Andreani C, Vale G, Berto S, Melegari M, Crouch AC, et al. Targeting de novo
865 lipogenesis and the Lands cycle induces ferroptosis in KRAS-mutant lung cancer. Nat Commun.
866 2022 Jul 26;13(1):4327.

867 50. She K, Fang S, Du W, Fan X, He J, Pan H, et al. SCD1 is required for EGFR-targeting cancer
868 therapy of lung cancer via re-activation of EGFR/PI3K/AKT signals. Cancer Cell Int. 2019
869 Dec;19(1):1–11.

870 51. Tracz-Gaszewska Z, Dobrzyn P. Stearoyl-CoA Desaturase 1 as a Therapeutic Target for the
871 Treatment of Cancer. Cancers. 2019 Jul 5;11(7):948.

872 52. Tissue expression of SCD - Summary - The Human Protein Atlas [Internet]. [cited 2024 Feb 23].
873 Available from: https://www.proteinatlas.org/ENSG00000099194-SCD/tissue

874 53. Skrypek K, Balog S, Eriguchi Y, Asahina K. Inhibition of Stearoyl-CoA Desaturase Induces the
875 Unfolded Protein Response in Pancreatic Tumors and Suppresses Their Growth. Pancreas. 2021
876 Feb 1;50(2):219–26.

877 54. Li YL, Tian H, Jiang J, Zhang Y, Qi XW. Multifaceted regulation and functions of fatty acid
878 desaturase 2 in human cancers. Am J Cancer Res. 2020 Dec 1;10(12):4098–111.

879 55. Xuan Y, Wang H, Yung MM, Chen F, Chan WS, Chan YS, et al. SCD1/FADS2 fatty acid
880 desaturases equipoise lipid metabolic activity and redox-driven ferroptosis in ascites-derived
881 ovarian cancer cells. Theranostics. 2022 Apr 24;12(7):3534–52.

882 56. Wang J, Liang H, Sun M, Zhang L, Xu H, Liu W, et al. Delta-6-desaturase inhibitor enhances
883 radiation therapy in glioblastoma in vitro and in vivo. Cancer Manag Res. 2018 Dec 7;10:6779–90.

884 57. He C, Qu X, Wan J, Rong R, Huang L, Cai C, et al. Inhibiting Delta-6 Desaturase Activity
885 Suppresses Tumor Growth in Mice. PLOS ONE. 2012 Oct 24;7(10):e47567.

886 58. Hasegawa K, Fujimori H, Nakatani K, Takahashi M, Izumi Y, Bamba T, et al. Delta-6 desaturase
887 FADS2 is a tumor-promoting factor in cholangiocarcinoma. Cancer Sci [Internet]. 2024 Aug 7
888 [cited 2024 Sep 12]; Available from: https://onlinelibrary.wiley.com/doi/abs/10.1111/cas.16306

889 59. Hansen-Petrik MB, McEntee MF, Johnson BT, Obukowicz MG, Masferrer J, Zweifel B, et al.
890 Selective inhibition of Δ-6 desaturase impedes intestinal tumorigenesis. Cancer Lett. 2002 Jan
891 25;175(2):157–63.

892 60. Ikeda T, Katoh Y, Hino H, Seta D, Ogawa T, Iwata T, et al. FADS2 confers SCD1 inhibition
893 resistance to cancer cells by modulating the ER stress response. Sci Rep. 2024 Jun 7;14(1):13116.

894 61. Vockley J. Optimizing metabolism is a complex issue. Nat Metab. 2024 Jan 19;1–2.

895 62. Fischer E, Sauer U. Large-scale in vivo flux analysis shows rigidity and suboptimal performance
896 of Bacillus subtilis metabolism. Nat Genet. 2005 Jun;37(6):636–40.

897 63. Qin C, Yang G, Yang J, Ren B, Wang H, Chen G, et al. Metabolism of pancreatic cancer: paving
898 the way to better anticancer strategies. Mol Cancer. 2020 Mar 2;19(1):50.

899 64. Cerone M, Smith TK. Desaturases: Structural and mechanistic insights into the biosynthesis of
900 unsaturated fatty acids. Iubmb Life. 2022 Nov;74(11):1036–51.

901 65. Guillou H, D'Andrea S, Rioux V, Barnouin R, Dalaine S, Pedrono F, et al. Distinct roles of
902 endoplasmic reticulum cytochrome b5 and fused cytochrome b5-like domain for rat Δ6-desaturase
903 activity. J Lipid Res. 2004 Jan 1;45(1):32–40.

904 66. Son J, Lyssiotis CA, Ying H, Wang X, Hua S, Ligorio M, et al. Glutamine supports pancreatic
905 cancer growth through a KRAS-regulated metabolic pathway. Nature. 2013 Apr 4;496(7443):101–
906 5.

907 67. Piccolis M, Bond LM, Kampmann M, Pulimeno P, Chitraju C, Jayson CBK, et al. Probing the
908 Global Cellular Responses to Lipotoxicity Caused by Saturated Fatty Acids. Mol Cell. 2019 Apr
909 4;74(1):32-44.e8.

910 68. Sánchez-Martínez R, Cruz-Gil S, de Cedrón MG, Álvarez-Fernández M, Vargas T, Molina S, et al.
911 A link between lipid metabolism and epithelial-mesenchymal transition provides a target for colon
912 cancer therapy. Oncotarget. 2015 Oct 5;6(36):38719–36.

913 69. Giudetti AM, De Domenico S, Ragusa A, Lunetti P, Gaballo A, Franck J, et al. A specific lipid
914 metabolic profile is associated with the epithelial mesenchymal transition program. Biochim
915 Biophys Acta BBA - Mol Cell Biol Lipids. 2019 Mar 1;1864(3):344–57.

916 70. Lee HJ, Chen Z, Collard M, Chen F, Chen JG, Wu M, et al. Multimodal Metabolic Imaging Reveals
917 Pigment Reduction and Lipid Accumulation in Metastatic Melanoma. BME Front. 2021:9860123.

918 71. Schwab A, Rao Z, Zhang J, Gollowitzer A, Siebenkäs K, Bindel N, et al. Zeb1 mediates
919 EMT/plasticity-associated ferroptosis sensitivity in cancer cells by regulating lipogenic enzyme
920 expression and phospholipid composition. Nat Cell Biol. 2024 Jul 15;1–12.

921 72. Afanas'ev I. Reactive Oxygen Species Signaling in Cancer: Comparison with Aging. Aging Dis.
922 2010 Feb 20;2(3):219–30.

923 73. Abdel Hadi N, Reyes-Castellanos G, Carrier A. Targeting Redox Metabolism in Pancreatic Cancer.
924 Int J Mol Sci. 2021 Feb 3;22(4):1534.

925 74. Magtanong L, Ko PJ, To M, Cao JY, Forcina GC, Tarangelo A, et al. Exogenous Monounsaturated
926 Fatty Acids Promote a Ferroptosis-Resistant Cell State. Cell Chem Biol. 2019 Mar 21;26(3):420-
927 432.e9.

928 75. Tesfay L, Paul BT, Konstorum A, Deng Z, Cox AO, Lee J, et al. Steroyl-CoA Desaturase 1 (SCD1)
929 protects ovarian cancer cells from ferroptotic cell death. Cancer Res. 2019 Oct 15;79(20):5355–66.

930 76. Zheng W, Xu S. Analysis of Differential Expression Proteins of Paclitaxel-Treated Lung
931 Adenocarcinoma Cell A549 Using Tandem Mass Tag-Based Quantitative Proteomics.
932 OncoTargets Ther. 2020 Oct 13;13:10297–313.

933 77. Guillou H, Martin PGP, Pineau T. Transcriptional Regulation of Hepatic Fatty Acid Metabolism.
934 In: Quinn PJ, Wang X, editors. Lipids in Health and Disease [Internet]. Dordrecht: Springer

Netherlands; 2008 [cited 2024 Feb 23]. p. 3–47. (Subcellular Biochemistry). Available from: https://doi.org/10.1007/978-1-4020-8831-5_1

78. Triki M, Rinaldi G, Planque M, Broekaert D, Winkelkotte AM, Maier CR, et al. mTOR Signaling and SREBP Activity Increase FADS2 Expression and Can Activate Sapienate Biosynthesis. Cell Rep. 2020 Jun 23;31(12):107806.

79. Abbott SK, Jenner AM, Mitchell TW, Brown SHJ, Halliday GM, Garner B. An Improved High-Throughput Lipid Extraction Method for the Analysis of Human Brain. Lipids. 2013 Mar 1;48(3):307–18.

80. Norris SE, Friedrich MG, Mitchell TW, Truscott RJW, Else PL. Human prefrontal cortex phospholipids containing docosahexaenoic acid increase during normal adult aging, whereas those containing arachidonic acid decrease. Neurobiol Aging. 2015 Jan;36(4):1659–69.

81. Jayashankar V, Selwan E, Hancock SE, Verlande A, Goodson MO, Eckenstein KH, et al. Drug-like sphingolipid SH-BC-893 opposes ceramide-induced mitochondrial fission and corrects diet-induced obesity. EMBO Mol Med. 2021 Jul 7;e13086.

82. Hu C, van Dommelen J, van der Heijden R, Spijksma G, Reijmers TH, Wang M, et al. RPLC-Ion-Trap-FTMS Method for Lipid Profiling of Plasma: Method Validation and Application to p53 Mutant Mouse Model. J Proteome Res. 2008 Nov 7;7(11):4982–91.

83. Bird SS, Marur VR, Sniatynski MJ, Greenberg HK, Kristal BS. Serum Lipidomics Profiling Using LC–MS and High-Energy Collisional Dissociation Fragmentation: Focus on Triglyceride Detection and Characterization. Anal Chem. 2011 Sep 1;83(17):6648–57.

84. Turner N, Lim XY, Toop HD, Osborne B, Brandon AE, Taylor EN, et al. A selective inhibitor of ceramide synthase 1 reveals a novel role in fat metabolism. Nat Commun. 2018 Aug 21;9(1):3165.

85. Tsugawa H, Cajka T, Kind T, Ma Y, Higgins B, Ikeda K, et al. MS-DIAL: data-independent MS/MS deconvolution for comprehensive metabolome analysis. Nat Methods. 2015 Jun;12(6):523–6.

86. Folch J, Lees M, Sloane Stanley GH. A simple method for the isolation and purification of total lipides from animal tissues. J Biol Chem. 1957 May;226(1):497–509.

87. Bollinger JG, Thompson W, Lai Y, Oslund RC, Hallstrand TS, Sadilek M, et al. Improved Sensitivity Mass Spectrometric Detection of Eicosanoids by Charge Reversal Derivatization. Anal Chem. 2010 Aug 15;82(16):6790–6.

88. Poad BLJ, Green MR, Kirk JM, Tomczyk N, Mitchell TW, Blanksby SJ. High-Pressure Ozone-Induced Dissociation for Lipid Structure Elucidation on Fast Chromatographic Timescales. Anal Chem. 2017 Apr 4;89(7):4223–9.